Inorganic Chemistry Communications 189 (2026) 116782

Contents lists available at ScienceDirect

Inorganic Chemistry Communications

journal homepage: www.elsevier.com/locate/inoche

Research Article

Neutralizing copper(II) complex charge through sulfonation: no1py2pyS as a new chelator for ^{64}Cu radiopharmaceuticals

Matteo Mari [a], Véronique Patinec [b], Raúl Alvarado [c], Sara Franchi [d], Marianna Tosato [e,f,g], Mattia Asti [e], Elia Frignani [a], Laura Pigani [a], Jennifer Storchi [a], Sven Stadlbauer [h], Constantin Mamat [h], Klaus Kopka [h,i], Marie Dallon [j], Carlos Platas-Iglesias [c], Raphaël Tripier [b,*], Erika Ferrari [a,*]

[a] Department of Chemical and Geological Sciences, University of Modena and Reggio Emilia, 41125 Modena, Italy
[b] Univ Brest, UMR CNRS 6521 CEMCA (Chimie et Electrochimie Moléculaires, Chimie Analytique), F29200 Brest, France
[c] CICA - Universidade da Coruña, Centro de Interdisciplinar de Química e Bioloxía and Departamento de Química, Facultade de Ciencias, 15071, A Coruña, Galicia, Spain
[d] Department of Chemical Sciences, University of Padova, 35131 Padova, Italy
[e] Radiopharmaceutical Chemistry Laboratory, Nuclear Medicine Unit, AUSL-IRCCS Reggio Emilia, 42122 Reggio Emilia, Italy
[f] Department of Chemistry, Simon Fraser University, Burnaby, V5A 1S6, British Columbia, Canada
[g] Life Sciences, TRIUMF, Vancouver, BC V6T 2A3, British Columbia, Canada
[h] Institut für Radiopharmazeutische Krebsforschung, Helmholtz-Zentrum Dresden-Rossendorf, D-01328 Dresden, Germany
[i] School of Science, Faculty of Chemistry and Food Chemistry, Technische Universität Dresden, Mommsenstraße 4, 01069 Dresden, Germany
[j] Univ Rennes, UMR CNRS 6226 ISCR (Institut des Sciences Chimiques de Rennes), F-35000 Rennes, France

ARTICLE INFO

Keywords:
Copper-64
TACN-based chelators
Radiopharmaceuticals
Theranostics
Polyazamacrocycles

ABSTRACT

We report the synthesis and comprehensive characterization of a novel sulfonated TACN-based ligand, no1py2pyS (L^{2S}), designed to combine high aqueous solubility, neutral complex charge, and strong Cu(II) affinity. L^{2S} was synthesized *via* an orthoamide pathway coupled with regioselective sulfonation of picolyl pendants. Protonation equilibria were investigated using ^{1}H NMR and UV–Vis spectroscopies. The Cu(II) complex ([CuL^{2S}]) formed rapidly under acidic (1 M HCl) and physiological (PBS, pH 7) conditions and remained stable across a wide pH range (0−12), even under highly acidic environment (5 M HCl). DFT calculations revealed two diastereoisomeric forms, Δ(λλλ) and Λ(λλλ), with a negligible free energy difference (0.04 kcal mol^{-1}), suggesting significant population of both forms at room temperature. However, EPR spectroscopy indicated the predominance of the Δ(λλλ)/Λ(δδδ) enantiomeric pair (87%), which displays a Jahn-Teller distorted octahedral geometry. X-ray crystallography validated the structure, revealing macrocyclic and pendant arm coordination (N_6 donor set) and sulfonate-mediated copper bridging. Cyclic voltammetry demonstrated quasi-reversible redox behavior, a reduction potential ($E_{1/2} = -614$ mV *vs.* Ag/AgCl/ 3 M KCl) below the physiological threshold and a reduced risk of demetallation, as no complex dissociation was observed. Finally, radiolabeling studies with [^{64}Cu]Cu^{2+} showed quantitative incorporation (>99%) under mild conditions (pH 4.5, RT, 10 min) at low concentration (10^{-6} M), and high stability in human serum for up to 2 h. Taken together, these findings identify L^{2S} as a promising platform for the development of copper-based radiopharmaceuticals.

1. Introduction

The use of theranostics represents an emerging approach in nuclear medicine that applies a single chemical tool for both diagnosis and therapy. In principle, it provides a range of advantages compared to conventional treatments, by facilitating patient selection for therapy, dosimetry calculations and assessment of treatment response [1]. The positron-emitting copper radioisotopes, copper-64 (^{64}Cu, $t_{1/2} = 12.7$ h) and copper-61 (^{61}Cu, $t_{1/2} = 3.33$ h), and the β^--emitter copper-67 (^{67}Cu, $t_{1/2} = 2.58$ d), form an attractive theranostic set that is gaining prominence in nuclear medicine for both diagnostic imaging and targeted radionuclide therapy. Among them, copper-64 [2–4] and copper-67 [5]

* Corresponding authors.
E-mail addresses: raphael.tripier@univ-brest.fr (R. Tripier), erika.ferrari@unimore.it (E. Ferrari).

https://doi.org/10.1016/j.inoche.2026.116782
Received 26 February 2026; Received in revised form 21 April 2026; Accepted 30 April 2026
Available online 6 May 2026

are already well established, with [^{64}Cu]Cu-DOTATATE providing substantially superior lesion detection of neuroendocrine tumors compared to [^{68}Ga]Ga-DOTATOC [6,7] using positron emission tomography (PET). The success of copper-based theranostics however critically depends on the design of chelators that ensure strong, selective binding and efficient delivery of the radiometal to its biological target [8]. Polyazamacrocycles have been extensively investigated in this context, with intense efforts focused on tuning redox behavior, ring size, denticity, and donor character to optimize stability and *in vivo* performances [9–13]. Classical carboxylated chelators based on cyclen (1,4,7,10-tetrazacyclododecane) and cyclam (1,4,8,11-tetraazacyclotetradecane), such as H_4DOTA and H_4TETA (Fig. 1), do not exhibit the required stability for *in vivo* applications. Cyclam cross-bridged derivatives such as H_2CB-TE2A and HCB-TE1PA (Fig. 1) show greater stability and might be compatible with *in vivo* applications, but their radiolabeling requires harsh conditions incompatible with thermosensitive targeting units such as antibodies [14,15]. TACN-based chelators, including 1,4,7-triazacyclononane-1,4,7-triacetic acid (NOTA) and ((7-(1-carboxy)-4-carboxybutyl)-1,4,7-triazacyclononane)-1,4-diacetic acid (NODAGA), together with DiamSar (Fig. 1), allow rapid radiolabeling under mild conditions while preserving outstanding *in vivo* stability, and are therefore considered the gold standard for radioactive copper chelation [13,16,17] However, the irreversibility of the redox process (Cu(II) ➔ Cu(I)) suggests a potential risk of metal release in highly reductive tumour micro environment, such as for DiamSar [16].

TACN-based Cu(II)-complexes generally show higher thermodynamic stability than their cyclen- and cyclam- counterparts (*e.g.*, pCu^{2+} = 16.2 (H_4TETA), 17.4 (H_4DOTA), 18.2 (H_3NOTA), at pH 7.4, C_L = 10 μM; C_{Cu}^{2+} = 1 μM) [13,18–20]. As demonstrated by Tosato et al., this enhanced performance is largely independent on the pendant arms, with the TACN backbone consistently improving the radiolabeling efficacy and stability in human serum [4,13]. In particular, picolyl *N*-functionalized TACN chelators such as no3py (L^{3py}) and Hno2py1pa (HL^{1PA}) (Fig. 1) combine high thermodynamic stability, kinetic inertness, efficient ^{64}Cu incorporation under mild conditions and a *quasi*-reversible electrochemical redox process, suggesting their ability to retain copper *in vivo* across the +2 and + 1 oxidation states [21,22]. However, their Cu(II) complexes remain positively charged, a feature that has been associated with less favorable biodistribution and increased non-specific interactions *in vivo*, as illustrated by the improved biodistribution of neutral NOTA-based systems [23].

Furthermore, recent advances in coordination chemistry have highlighted the benefits of incorporating sulfonic groups into ligand frameworks to enhance metal complex stability, solubility, and selectivity.

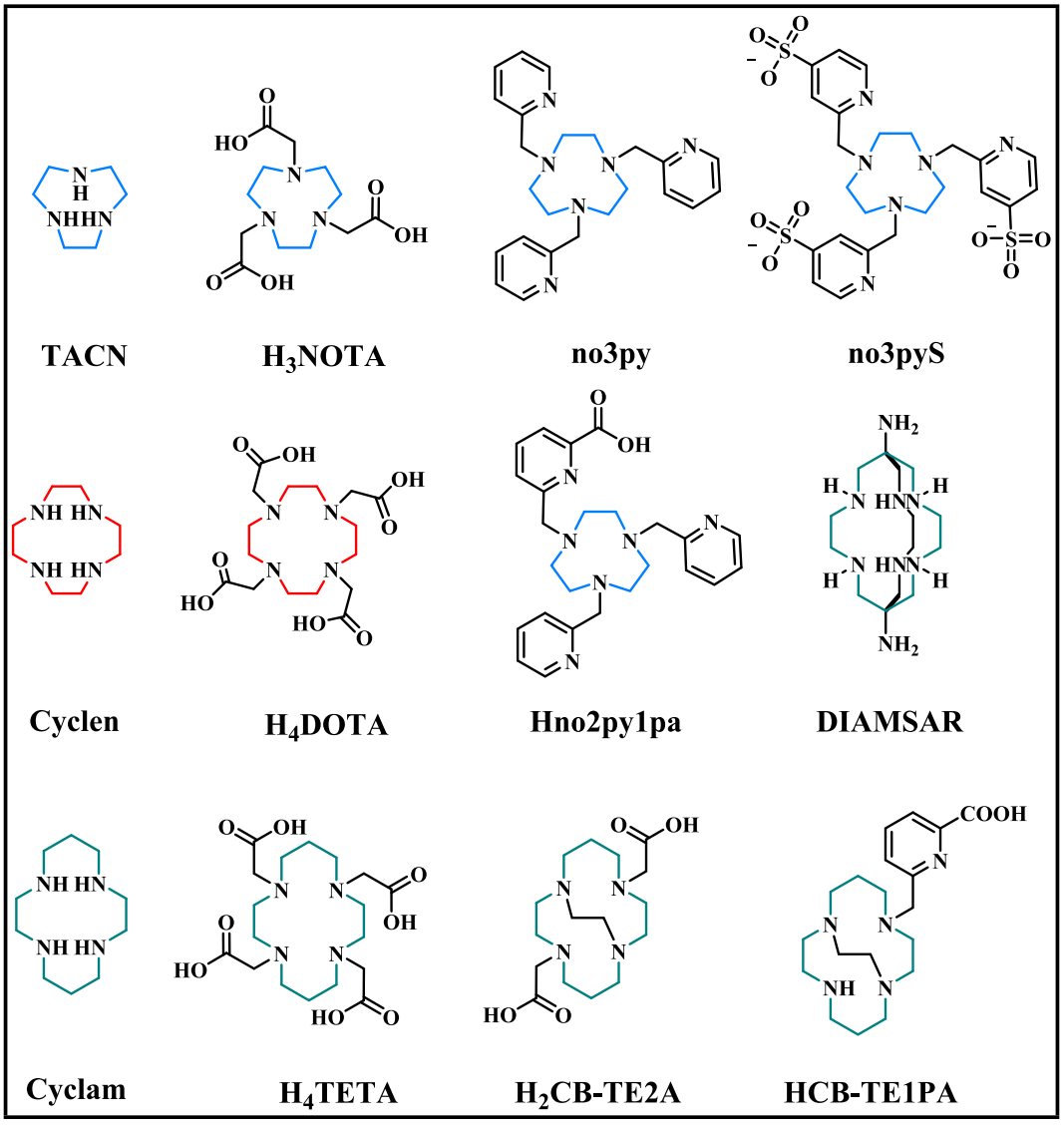

Fig. 1. Examples of polyazamacrocycles for Cu(II) chelation discussed in this paper.

Sulfonated *N,O*-chelating ligands, such as those used in arene Ru(II) complexes, have demonstrated improved biological activity, including enhanced cytotoxicity and antibacterial effects, compared to their non-sulfonated counterparts [24,25]. In antiviral applications, sulfonated polyanionic ligands like ethylenediamine-N,N,N′,N′-tetraethanesulfonate (edts) have shown dual activity against HIV, acting both pre- and post-infection, especially when coordinated with transition metal cations such as Ni(II), Co(II), Cu(II), and Zn(II) [26].

Among sulfonated macrocyclic ligands, 1,4,7-tris-(4-sulfonate-picolyl)-1,4,7-triazacyclononane (H_3no3pyS, L^{3S}) stands out as a promising scaffold (Fig. 1). Synthesized and investigated by Salaam et al. [27], this chelator - classified as a sulfonated no3py derivative - was designed to yield highly water-soluble metal complexes with Fe(II) (low spin) and Zn(II). Notably, the Fe(II) complex exhibited reduced cytotoxicity toward mammalian cells compared to the analogous Fe(II)-no3py complex, suggesting that sulfonation may mitigate biological toxicity while preserving metal-binding efficiency.

In addition to enhancing aqueous solubility, sulfonic functionalization offers an effective strategy to modulate the global charge of metal complexes, thereby limiting undesirable interactions with the targeting vector moiety and improving their compatibility with biological environments. When combined with a high-performance chelating platform such as no3py, sulfonic groups open the possibility of achieving a finely balanced system that couples strong Cu(II) coordination with excellent solubility and a tunable overall charge, an advantage that classical architectures such as H_3NOTA cannot readily offer.

On this basis, the present work was guided by three main design objectives: (1) to neutralize the overall charge of the Cu(II) complex at physiological pH through the introduction of sulfonic groups;

(2) to preserve the favorable thermodynamic stability, kinetic inertness, and redox behavior characteristic of picolyl-functionalized TACN chelators such as no3py; and (3) to achieve efficient ^{64}Cu radiolabeling under mild conditions, outperforming clinically relevant TACN-based benchmarks such as NODAGA, particularly at low ligand concentrations.

In this context, we introduce the new no3py-based chelator **no1py2pyS** (L^{2S}, Fig. 2) - synthesized here for the first time and fully characterized - featuring two *para*-sulfonated picolyl arms able to neutralize the overall metal-complex charge. Its coordination properties toward Cu(II) were examined through detailed thermodynamic studies of the Cu^{2+}–L^{2S} system. UV–Vis and EPR spectroscopies, supported by DFT calculations, provided further insight into the geometry and electronic structure of the complex, while cyclic voltammetry revealed its redox behavior relevant to *in vivo* stability. Finally, the radiolabeling performance of L^{2S} with [^{64}Cu]Cu(II) was assessed and benchmarked against gold standard chelators, highlighting its potential in radiopharmaceutical applications.

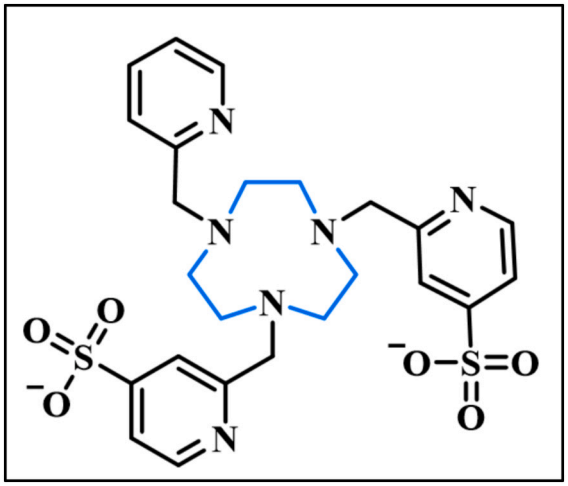

Fig. 2. Chemical structure of the TACN-based polyazamacrocycle **no1py2pyS** (L^{2S}).

2. Experimental

2.1. General

All chemicals were obtained from commercial suppliers and used as received without further purification. All solutions were prepared with ultrapure water (18.2 MΩ·cm) obtained from a Milli-Q Millipore system. Flash column chromatography was performed using silica gel (60 Å, 230–400 mesh, 40–63 μm, Sigma-Aldrich) and appropriate mobile phases, as described in the following section. NMR spectra were recorded on a Bruker Avance AMX 400 spectrometer (400.12 MHz ^{1}H; 100.13 MHz ^{13}C), Bruker Avance AMX 500 spectrometer (500.13 MHz ^{1}H; 126.13 MHz ^{13}C) or a Bruker Avance AMX 600 spectrometer equipped with a CryoProbe BBO H&F 5 mm in inverse detection (600.13 MHz ^{1}H, 150.13 MHz ^{13}C). All the NMR spectra were acquired at 298 K. Chemical shifts (δ) are reported in parts per million (ppm), referenced to the residual solvent peak in organic solvents or 3-(trimethylsilyl)propionic acid sodium salt (TSP) in D_2O. Coupling constants (J) are given in hertz (Hz). ^{1}H and ^{13}C NMR spectra of all intermediates and final product (L^{2S}) together with atom numbering are reported in the Supplementary Information (**Figs. S1-S7**). Mass spectrometry (MS) was performed on an Agilent 6300 Ion Trap LC-MS system with an electrospray ionization (ESI) interface. Elemental analyses were carried out using a Thermo Scientific™ FLASH 2000 CHNS Analyzer. UV–Vis spectra were recorded on a JASCO V-770 UV/Vis/NIR spectrophotometer within the 200–700 nm spectral range, using quartz cells (1 cm optical path). The inductively coupled plasma mass spectra (ICP-MS) were acquired with the spectrometer iCAP TQ ICP-MSX (Thermo Fisher Scientific) equipped with Peltier cooled (3 °C) spray chamber. Samples were mineralized with sub-boiling HNO_3, diluted with Milli-Q water to a final concentration of 200–500 ppb and then introduced by the autosampler ESI SC-2 DX FAST into the nebulizer. Data were analyzed by Qtegra software. The instrument was tuned daily with an ICP-MS tuning solution. Electron paramagnetic resonance (EPR) spectra were recorded with a Bruker Elexsys 500 instrument, in a 0.5 mm capillary within a quartz tube, at 9.34 GHz (band X). Measurements were conducted on frozen DMF/H_2O (1,1) solutions of the metal complex (C_{CuL} = 1.0 mM, 77 K). Simulations of the EPR spectra were performed using Easyspin [28] and Simultispin [29] softwares. Electrochemical measurements were carried out as previously reported [30].

2.2. Synthesis

4-Chloropyridin-2-yl)methanol (1). Compound **1** was obtained following the synthesis reported by Salaam et al. [27]. Briefly, methyl 4-chloropicolinate (3.108 g, 17.26 mmol) was dissolved in methanol (MeOH, 20 mL). Sodium borohydride (3.046 g, 80.52 mmol) was added in small portions while stirring and cooling the mixture with an ice bath (0 °C). The solution was then left under magnetic stirring at room temperature (RT) overnight. Water was added to quench the reaction and MeOH was then removed under reduced pressure. The mixture was extracted four times with ethyl acetate. The organic fractions were recollected, washed with brine, dried under $MgSO_4$, filtered off and the solvent was removed under reduced pressure. The product was collected as a white solid (yield 91%). Elemental analysis for C_6H_6ClNO (143.57 g/mol) experimental (calculated): C % 49.95 (50.20%), H % 4.40 (4.21%), N % 9.69 (9.76%).^{1}H NMR (400 MHz, $CDCl_3$) δ (ppm): 3.2 (s, 1H, -OH), 4.8 (s, 2H, H-1), 7.2 (dd, J = 5.3, 2.0 Hz, 1H, H-5), 7.3 (d, J = 2.0 Hz, 1H, H-3), 8.5 (d, J = 5.4 Hz, 1H, H-6). ^{13}C NMR ($CDCl_3$, 400 MHz) δ (ppm): 161.2 (C-2), 149.5 (C-6), 145.1 (C-4), 123.0 (C3/5), 121.1 (C-3/5), 64.1 (C-1). ESI-MS: m/z 144.2 [^{35}Cl-M + H]$^+$ (found), 144.02107 (calc. For $C_6H_7^{35}ClNO^+$); 146.0 [^{37}Cl-M + H]$^+$ (found),

146.02107 (calc. For $C_6H_7^{37}ClNO^+$).

4-Chloro-2-(chloromethyl)pyridine (2). Following the synthesis reported by Salaam et al. [27], compound **1** (941 mg, 6.58 mmol) was dissolved in dichloromethane (DCM, 30 mL) and $SOCl_2$ (0.7 mL, 9.63 mmol in 10 mL of DCM) was slowly added under stirring and cooling with an ice-bath (0 °C) for 1 h. The solution was then allowed to warm to room temperature and stirred for 2 h. The reaction was then quenched with ethanol (EtOH) and the solvent was removed under reduced pressure. The product was isolated as the hydrochloride salt ($C_6H_5Cl_2N{\cdot}HCl$) as a white powder (yield 100%). Elemental analysis for $C_6H_5Cl_2N{\cdot}HCl$ (162.013 g/mol) experimental (calculated): C % 44.29 (44.48%), H % 3.45 (3.11%), N % 8.51 (8.65%). ^{1}H NMR (400 MHz, $CDCl_3$) δ 4.7 (s, 2H, H-1), 7.3 (d, $J = 6.7$ Hz, 2H, H-5), 7.5 (d, $J = 1.9$ Hz, 1H, H-4), 8.5 (dd, $J = 5.4$, 0.6 Hz, 1H, H-6). ^{13}C NMR (400 MHz, $CDCl_3$) δ 158.2 (C-2), 150.3 (C-6), 145.3 (C-4), 123.6 (C-3/5), 123.3 (C-3/5), 46.0 (C-1). ESI-MS: *m/z* 162.1 $[^{35}Cl\text{-}M + H]^+$ (found), 161.98718 (calc. For $C_6H_6^{35}Cl_2N^+$); 164.0 $[^{37}Cl\text{-}M + H]^+$ (found), 163.98718 (calc. For $C_6H_6^{37}Cl_2N^+$).

1,4,7-Triazacyclononane(TACN)-orthoamide (3). TACN (1.075 g, 8.32 mmol) was dissolved in dry DCM (4 mL) and diluted in dry toluene (16 mL). 1,1-Dimethoxy-*N*,*N*-dimethylmethanamine (1.5 mL, 1.09 mmol) was then added, and the mixture was kept under magnetic stirring at room temperature overnight. The solvent was removed under reduced pressure. The product was isolated as a colorless oil (yield 95%). ^{1}H NMR (400 MHz, $CDCl_3$) δ (ppm): 2.7–2.9 (m, 6H, H-1′), 3.1 (m, 6H, H-1), 4.9–5.1 (m, 1H, H-2). ^{13}C NMR (400 MHz, $CDCl_3$) δ (ppm): 104.2 (C-2), 52.0 (C-1). ESI-MS: *m/z* 140.2 $[M + H]^+$ (found), 140.11822 (calc. For $C_7H_{14}N_3^+$).

2a-[(Pyridin-2-yl)methyl] hexahydro-6bH-2a,4a,6a-triazacyclopenta[*cd*]pentalene chloride (4). Compound **3** was dissolved in chloroform ($CHCl_3$, 3 mL), then dry tetrahydrofuran (THF (20 mL) was added. 2-(Chloromethyl)pyridine was added, and the mixture was left stirring at RT for 7 days. A white precipitate formed, the supernatant was removed, and the precipitate was washed three times with dry THF. The product was isolated as a highly hygroscopic white solid (yield 65%). ^{1}H NMR (400 MHz, D_2O) δ (ppm): 3.2 (m, 4H, H-1), 3.5 (m, 6H, H-2 and H-3), 4.05 (m, 2H, H-3′), 4.7 (s, 2H, H-4), 6.0 (s, 1H, H-10), 7.55 (m, 1H, H-8), 7.7 (m, 1H, H-6), 7.95 (m, 1H, H-7), 8.65 (m, 1H, H-9). ^{13}C NMR (400 MHz, D_2O) δ 149.9 (C-9), 148.1 (C-5), 138.8 (C-7), 127.5 (C-6/8), 125.6 (C-6/8), 117.9 (C-10), 62.6 (C-4), 58.1 (C-3), 53.7 (C-1/2), 51.1 (C-1/2). ESI-MS: *m/z* 231.2 $[M]^+$ (found), 231.16096 (calc. For $C_{13}H_{19}N_4^+$).

1-(2-Picolinyl)-1,4,7-triazacyclononane (5). Compound **4** (345 mg, 1.29 mmol) was dissolved in 6 M HCl (30 mL) and the mixture was stirred at room temperature overnight. KOH was then added until a pH of 13–14 was reached. The basic aqueous solution was extracted three times with $CHCl_3$. The organic fractions were recollected, washed with brine, dried with $MgSO_4$ and the solvent removed under reduced pressure. A yellow oil was obtained (yield 100%). ^{1}H NMR (400 MHz, $CDCl_3$) δ (ppm): 2.7 (s, 8H), 2.9 (s, 4H), 3.5 (s, 4H), 3.9 (s, 2H), 7.2 (ddd, $J = 7.6$, 4.9, 1.2 Hz, 1H), 7.4 (dd, $J = 7.8$, 1.3 Hz, 1H), 7.6 (td, $J = 7.7$, 1.8 Hz, 1H), 8.6 (ddd, $J = 4.9$, 1.9, 0.9 Hz, 1H). ^{13}C NMR (400 MHz, $CDCl_3$) δ (ppm): 159.7 (C-5), 149.3 (C-9), 136.8 (C-7), 123.1 (C-6/8), 122.3 (C-6/8), 62.2 (C-4), 53.0 (C-3), 46.9 (C-1/2), 46.5 (C-1/2). ESI-MS: *m/z* 221.1 $[M + H]^+$(found), 221.17607 (calc. For $C_{12}H_{21}N_4^+$).

1,4-Di[(4-chloropyridin-2-yl)methyl]-7-[(pyridin-2-yl) methyl]-1,4,7-triazonane (6). Compound **5** (278 mg, 1.26 mmol) was dissolved in dry acetonitrile (20 mL). K_2CO_3 was added and the mixture was stirred at room temperature for 30 min. Compound **2** (647 mg, 3.28 mmol) was suspended in dry acetonitrile (20 mL) and added to the first solution. The mixture was kept under stirring for 3 days at RT. The mixture was dried under reduced pressure. The sticky solid was then suspended with DCM, impurities were filtered off and the organic phase was washed with water and brine. The organic phase was then dried with $MgSO_4$, filtered off and the solvent removed under reduced pressure. The crude yellow oil was used without further purification (yield 95%). Elemental analysis for $C_{24}H_{28}Cl_2N_6$ (470.175 g/mol) experimental (calculated): C % 60.97 (61.15%), H % 6.12 (5.99%), N % 17.77 (17.83%). ^{1}H NMR (400 MHz, MeOD-d_4) δ (ppm): 2.9 (d, $J = 3.4$ Hz, 12H, H-1, H-2, H-3), 3.8 (d, $J = 3.6$ Hz, 6H, H-4, H-10), 7.3 (ddd, $J = 7.6$, 4.9, 1.2 Hz, 1H, H-8), 7.4 (dd, $J = 5.5$, 2.1 Hz, 2H, H-13), 7.6 (d, $J = 7.8$ Hz, 1H, H-6), 7.7 (d, $J = 2.1$ Hz, 2H, H-15), 7.8 (ddd, $J = 7.7$, 1.8 Hz, 1H, H-7), 8.4 (d, $J = 5.5$ Hz, 2H, H-12), 8.4–8.5 (m, 1H, H-9). ^{13}C NMR (400 MHz, MeOD-d_4) δ (ppm): 163.4 (C-11), 161.1 (C-5), 150.7 (C-12), 149.3 (C-9), 146.3 (C-14), 138.6 (C-7), 125.3 (C-6/8), 125.1 (C-13/15), 123.9 (C-13/15), 123.7 (C-6/8), 65.2 (C-4), 64.7 (C-10), 57.0 (C-1, C-2, C-3). MS (ESI): *m/z* 471.3 $[^{35}Cl\text{-}M + H]^+$ (found), 471.18252 (calc. For $C_{24}H_{29}^{35}Cl_2N_6^+$); 473.3 $[^{37}Cl\text{-}M + H]^+$ (found), 473.18252 (calc. For $C_{24}H_{29}^{37}Cl_2N_6^+$); 493.2 $[^{35}Cl\text{-}M + Na]^+$ (found), 493.16501 (calc. For $C_{24}H_{28}^{35}Cl_2N_6Na^+$); 495.3 $[^{37}Cl\text{-}M + Na]^+$ (found), 495.16501 (calc. For $C_{24}H_{28}^{37}Cl_2N_6Na^+$).

Di sodium 1,4-Bis(6-sulfonate-2-picolinyl)-7-(2-picolinyl)-1,4,7-triazacyclononane – no1py2pyS (L^{2S};7). Compound **6** (427 mg, 0.908 mmol) was dissolved in MeOH (25 mL). A solution of Na_2SO_3 (3.036 g, 23.26 mmol) in H_2O (25 mL) was added to the first solution. The mixture was refluxed for 30 days. The solvent was then evaporated. The solid was washed with ethanol and filtered off. The organic phase was then dried under reduced pressure. The crude product was purified with semi-preparative HPLC (mobile phase gradient: H_2O/ACN 98/2 *V*/V ➔ H_2O/ACN 10/90 *V*/V). The product was isolated as a yellow solid (yield 43%). Elemental analysis for $C_{24}H_{29}N_6NaO_6S_2 \cdot 2H_2O$ (620.170 g/mol) experimental (calculated): C 46.36% (46.44%), H 5.07% (5.36%), N 13.30% (13.54%), S 10.20 (10.33%). ^{1}H NMR (500 MHz, D_2O) δ (ppm): 3.0 (d, $J = 24.7$ Hz, 12H, H-1, H-2, H-3), 4.1 (s, 6H, H-4, H-10), 7.4 (m, 1H, H-8), 7.5 (dd, $J = 7.8$, 1.1 Hz, 1H, H-6), 7.7–7.8 (m, 2H, H-14), 7.8–7.8 (m, 1H, H-7), 7.8 (s, 2H, H-12), 8.5 (d, $J = 5.0$ Hz, 1H, H-9), 8.7 (d, $J = 5.2$ Hz, 2H, H-15). ^{13}C NMR (500 MHz, D_2O) δ (ppm): 159.6 (C-11), 156.6 (C-5), 154.7 (C-13), 153.1 (C-15), 151.7 (C-9), 141.2 (C-7), 127.8 (C-6/8), 126.9 (C-6/8), 122.9 (C-12/14), 122.3 (C-12/14), 63.0 (C-4), 62.7 (C-10), 52.6 (C_{TACN}), 52.2 (C_{TACN}), 51.7 (C_{TACN}). LC-MS (ESI): *m/z* 563.1741 $[M + H]^+$ (found), 563.17410 (calc. For $C_{24}H_{31}N_6O_6S_2^+$); 282.0914 $[M + 2H]^{2+}$ (found), 282.09124 (calc. For $C_{24}H_{32}N_6O_6S_2^{2+}$) (**Fig. S8**).

[CuL^{2S}]. Compound **7** (51.8 mg, 0.083 mmol) was dissolved in Milli-Q water (2.0 mL), then a 49.3 mM solution of $Cu(ClO_4)_2$ was added (1.87 mL, 0.092 mmol). The pH was adjusted to 7.0 with 1 M KOH. The solution was left under magnetic stirring at RT overnight. The solution was then dried, washed with MeOH twice and dried. A blue solid was obtained (yield 89%). Elemental analysis for $Cu_3C_{48}H_{66}N_{12}O_{17}S_4$ (1402.0 g/mol) experimental (calculated): C 41.09% (41.12%), H 4.79% (4.74%), N 11.94% (11.99%), S 8.83 (9.15%). LC-MS (ESI): *m/z* 624.089 $[M + H]^+$ (found), 624.09804 (calc. For $C_{24}CuH_{29}N_6O_6S_2^+$); 312.548 $[M + 2H]^{2+}$(found), 312.55321 (calc. For $CuC_{24}H_{30}N_6O_6S_2^{2+}$).

2.3. Kinetic experiments

Equimolar amounts of Cu^{2+} ($CuCl_2$) were added to solutions of the chelator ($C_{L^{2S}}$ = 0.1 mM) in either HCl (C_{HCl} = 2.5 M or 1.0 M) or phosphate buffered saline (PBS, 0.1 M, pH 7.4). The UV–Vis spectra were collected before the addition (free L^{2S}), immediately after and at different time points up to reaching a steady-state corresponding to the complete formation of the metal complex. The complexation reaction was monitored directly by following the increase of the ligand-to-metal charge transfer (LMCT) band (λ = 300 nm). The formation of Cu(II)-L^{2S} complex was investigated by absorption visible spectroscopy. Absorption spectra were acquired in the 500–800 nm range after the addition of increasing amounts of $CuCl_2$ (0.5 M) to L^{2S} solution (10 mM; 5 mL) until the Cu(II)/L^{2S} molar ratio of 1.5 was reached (PBS 0.1 M, pH 7.4).

The kinetic inertness of the metal complex [CuL^{2S}] in 1 M and 5 M HCl was investigated by UV–Vis spectroscopy (500–800 nm; d-d transition). A stock solution of [CuL^{2S}] (5 mM) was prepared by dissolving the solid complex [CuL^{2S}] in milli-Q water, with the initial pH of the

solution was ~7. An adequate amount of the CuL^{2S} stock solution and concentrated HCl (37% m/m) were diluted in milli-Q water to reach the final concentrations $C_{CuL^{2s}} = 0.1$ mM and $C_{HCl} = 1$ M (or 5 M). UV–Vis spectra were acquired from time zero up to 14 days.

2.4. Thermodynamic experiments

UV–Vis titrations were conducted using the in-cell method. The ligand molar concentration ($C_{L^{2s}}$) was 0.1 mM and small negligible volumes (μL) of HCl and/or NaOH were used to adjust the pH, that was measured using a combined glass electrode connected to a pH-meter (Mettler-Toledo). The system was calibrated and the absorption spectra were recorded at $T = 25$ °C and $I = 0.15$ M NaCl in the pH range 0–14. The equilibrium was considered to be reached when no further changes in either the pH or the electronic spectra were observed. Under highly acidic (pH <2) or basic (pH >12) conditions, batch solutions were prepared and the pH was calculated from the HCl/NaOH concentration using the formula $pH = -\log[C(H^+)]$.

^{1}H NMR pH-titrations were performed similarly to UV–Vis titrations. ^{1}H NMR spectra of the chelator in D_2O ($C_L = 4$ mM) were recorded at different pH ($T = 25$ °C; $I = 0.15$ M NaCl). The pH was adjusted following the procedure used in the UV–Vis experiments. To account for isotopic effects, 0.41 log units were added to the measured pH values [31]. The thermodynamic data were elaborated with HypSpec, HypNMR or as described in previous publications [4,32,33]. The wavelength range of UV–Vis spectra used for the calculation of protonation constants using HypSpec was 215–350 nm. Speciation diagrams were calculated using PyES [34].

2.5. X-ray crystallography

A suitable crystal for X-ray diffraction single crystal experiment (blue prism, dimensions = 0.080 × 0.200 × 0.500 mm) was selected and mounted on the goniometer head of a D8 Venture (Bruker-AXS) diffractometer equipped with a CMOS-PHOTON70 detector. Data were collected using Mo-Kα radiation (λ = 0.71073 Å, multilayer monochromator) at $T = 150(2)$ K. The compound crystallized in the centrosymmetric monoclinic space group C2/c (I.T.#15; Rint = 0.0317; Rsig = 0.0330). Cell parameters have been determined as follows: $a = 40.386(4)$, $b = 13.6096(15)$, $c = 11.5413(11)$ Å, $\beta = 95.588(4)$ °, V = 6313.3 (11) Å^3. The crystal structure was solved using a dual-space algorithm with the SHELXT program [35], and then refined with full-matrix least-squares methods based on F2 (SHELXL [36]).

2.6. DFT calculations

All quantum chemical calculations were performed using the ORCA 6.0 software package [37–39]. Density Functional Theory (DFT) was employed with the TPSSh hybrid meta-GGA functional in an unrestricted formalism (UKS), suitable for open-shell systems such as Cu(II) complexes. The def2-TZVPP basis set [40] was used for all atoms, along with the D3 dispersion correction developed by Grimme [41,42] and a third-level integration grid (defgrid3). To accelerate the calculations, the RIJCOSX approximation [43–46] was applied with automatically generated auxiliary basis sets (autoaux) [47]. Tight SCF convergence criteria were adopted throughout. Vibrational frequency analysis was carried out analytically to confirm the nature of the optimized structures as true minima. No scaling factor was applied to the computed frequencies (ScalFreq = 1.0). Solvent effects were incorporated with solvation model based on density (SMD) developed by Truhlar [48,49]. Optimized Cartesian coordinates of the structures used in this work and a sample input file are provided in the Supplementary material (**Tables S1** and **S2**). The SHAPE 2.1 software was used to analyze the geometric distortion of the coordination polyhedron in the optimized geometries [50].

2.7. Copper-64 radiolabeling and stability under physiological conditions

Caution! ^{64}Cu emits ionizing radiation. It should be handled only by trained personnel in properly equipped facilities.

^{64}Cu was cyclotron-produced at Helmholtz-Zentrum Dresden-Rossendorf (Germany) through the ^{64}Ni(p,n)^{64}Cu reaction and subsequently isolated as [^{64}Cu]$CuCl_2$ in 0.05 M HCl. L^{2S} and NODAGA stock solutions were prepared in ultrapure metal-free water at 10^{-3} M and diluted appropriately to give a serial dilution series (10^{-4} - 10^{-6} M).

Radiolabeling experiments were performed by adding [^{64}Cu]$CuCl_2$ (1–3 MBq, 10 μL) to a solution containing the ligand (10 μL) at the appropriate concentration, along with a proper buffer depending on the desired final pH (pH 4.5: 80 μL 0.1 M sodium acetate; pH 7: 80 μL PBS 0.1 M). Reactions were conducted at room temperature (RT) or 90 °C for 10 min. All radiolabeling reactions were repeated at least three times.

Radiochemical incorporation (RCI) was determined *via* radio-thin layer chromatography (radio-TLC) on aluminum plates coated with silica gel 60 RP-18 F_{254}s (Merck) using a 0.1 M aqueous solution of sodium citrate as eluent. Under these conditions, free [^{64}Cu]Cu(II) migrates with the solvent front ($R_f = 1$) while [^{64}Cu]Cu^{2+} complexes remain at the baseline ($R_f = 0$). Radio-TLC were analyzed with an Amersham Typhoon 5 equipped with phosphor imaging plates (GE Healthcare) and RCI was determined with the program AIDA 5.10. The stability of the preformed complexes ([^{64}Cu][CuL^{2S}] and [^{64}Cu][Cu(NODAGA)]$^-$ as a reference) was evaluated over time by incubating them in human serum (1:1 *V/V* dilution) at $T = 37$ °C. The radiometal-complex stability was monitored over 2 h using radio-TLC, following the protocol described above.

3. Results and discussion

3.1. Synthesis

no1py2pyS (**L^{2S}**) was synthesized combining the renowned orthoamide pathway reported for asymmetrically substituted TACN-based chelators [12,21,51,52] with the sulfonation reaction for picolyl derivatives [27] (Fig. 3). The intermediate **6** - obtained through a 4-step process - was isolated with an overall yield around 60%. The limiting step is represented by the sulfonation of the chloro-activated picolyl rings. Indeed, this reaction, due to the weak nucleophilic strength of SO_3^{2-}, is extremely slow (30 days) and provides the final product in modest yield (43%). In comparison to no3py (briefly L^{3py} in the following discussion), **L^{2S}** is characterized by an asymmetric TACN substituted ring that accounts for the higher complexity of the ^{1}H NMR spectrum (**Fig. S7**) due to the three different pyridines that originate two sets of signals with 1-to-2 integrated area ratio. In D_2O (neutral pH), the protons belonging to the TACN backbone form a set of broad multiplets with close chemical shifts possibly due to the establishment of *intra/inter* molecular hydrogen bonds.

3.2. Acid-base behavior

The chelator L^{2S} is featured with a potential N_6 donor set associated to the three amine groups of TACN ring and the three picolyl arms. Sulfonic groups are not considered as they are deprotonated in a wide pH range (pK_a of *p*-Toluenesulfonic acid) = −2.8, implying a degree of dissociation of 99.84% at pH ~0 [53]), therefore a maximum of six acid-base equilibria can be expected. The protonation constants were estimated by ^{1}H NMR data and then complemented with electronic absorption spectroscopy (UV–Vis). The ^{1}HNMR pH-metric titration of L^{2S} shows that both aliphatic and aromatic signals undergo evident shifts upon changing the pH (Fig. 4**, Fig. S9**). In strong basic conditions (pH 9–12), the major shifts are observed for aliphatic signals while only minimal changes appear for aromatic protons, regardless of the presence of a sulfonic group. This suggests that protonation in this pH range occurs on an amine group of the macrocyclic ring. In the pH range 9–6, the

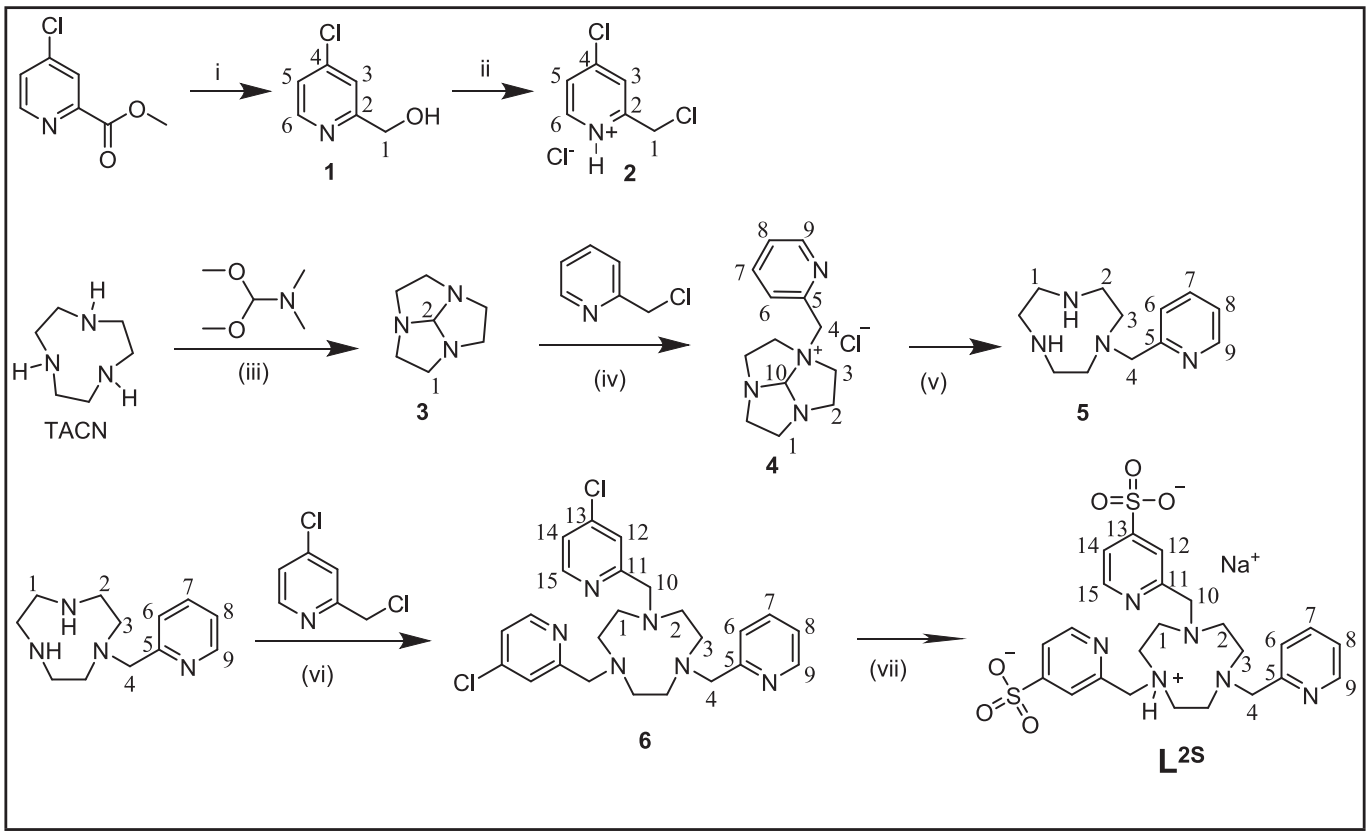

Fig. 3. Synthetic scheme of **no1py2pyS** (L^{2S}): (i) $NaBH_4$, MeOH, RT, 16 h; (ii) $SOCl_2$, DCM, 0 °C, 1 h ➔ RT, 3 h; (iii) DCM-Toluene, RT, 16 h; (iv) dry THF, RT, 3 d; (v) 6 M HCl, RT, 18 h, then NaOH pellets; (vi) K_2CO_3, ACN, RT, 3 d; (vii) Na_2SO_3, MeOH/H_2O 1:1, reflux, 30 d.

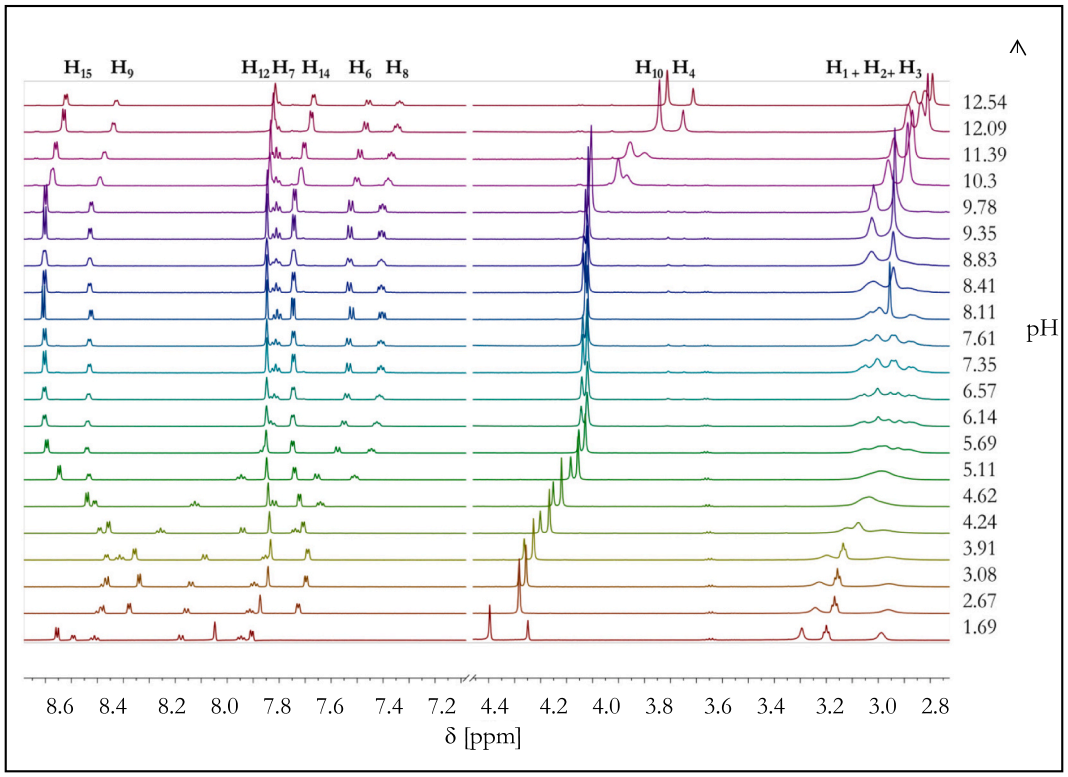

Fig. 4. ^1H NMR spectra of L^{2S} at different pH values together with signal attributions (600 MHz, D_2O, T = 25 °C, I = 0.10 M NaCl, $C_{L^{2S}}$ = 4.0 mM).

chemical shifts remain barely affected, with only TACN ethylene protons undergoing a slight line broadening. Below pH 5.7 both aromatic and

aliphatic protons experience significant shifts, suggesting the involvement of both the azamacrocycle and the aromatic units in the protonation process. In the pH range 6–4, the largest shifts are observed for the unsubstituted picolyl protons ($\Delta\delta_{H\text{-}6} = 0.584$ ppm; $\Delta\delta_{H\text{-}7} = 0.596$ ppm; $\Delta\delta_{H\text{-}8} = 0.438$ ppm) rather than the sulfonated ones ($\Delta\delta_{H\text{-}15} = 0.351$ ppm; $\Delta\delta_{H\text{-}12} = 0.013$ ppm; $\Delta\delta_{H\text{-}14} = 0.056$ ppm). Below pH 3, the opposite behavior is observed, as the aromatic protons of the sulfonated picolyl ring are more downfield shifted than those of the corresponding unsubstituted one. These results suggest that the sulfonation of the picolyl ring slightly reduces the basicity of the N atom. Below pH 2, all the aliphatic protons show separate and quite narrow signals. The proton dissociation constants (pK_a) calculated from ^{1}H NMR data are reported in Table 1, and commented below together with the values elaborated from spectrophotometric data.

The absorption spectra of L^{2S} at different pH (Fig. 5) are characterized by a maximum absorption at $\lambda_{max} = 263$ nm typical of the $\pi \rightarrow \pi^*$ transition of the pyridine rings, and a second band around 215 nm related to aliphatic amines but also affected by the presence of chloride ions in solution. As the pH increases, the pyridine band decreases in intensity while the maximum tends to flatten. A slight bathochromic shift of the maximum is observed in comparison to no3py (λ_{max} 260 nm), suggesting a mild effect of the sulfonic groups.

The pK_a values calculated from both NMR and UV–Vis data are summarized in Table 1 together with the corresponding values for no3py (L^{3py}) previously reported in literature [21,30]. The results obtained for L^{2S} are in line with those of L^{3py}, although only three out of four protonation constants were calculated. ^{1}H NMR and UV–Vis delivered consistent results. The slight discrepancy observed for $pK_{a,4}$ (corresponding to the first protonation of the TACN ring) is likely related to the use of Na^+ (NaCl) as background electrolyte. At the higher ligand concentrations required for ^{1}H NMR titrations, weak Na^+–ligand interactions may partially compete with protonation of the TACN amine, resulting in a lower apparent protonation constant compared to UV–Vis measurements. The pK_a of the first amine group of L^{2S} is considerably high and consistent with the reference compound L^{3py}. On the contrary, the second protonation of the TACN ring is hampered by the small ring size that results in high repulsion between two positively charged ammonium groups; as a consequence, more acidic conditions are required for the protonation to happen (below pH ~ 5). As suggested by the NMR data, the calculated $pK_{a,3}$ could be an average of two protonation equilibria that occur at very similar pH, one due to the protonation of a TACN amine and another one of the non-sulfonated picolyl nitrogen. The last calculated protonation ($pK_{a,2}$) can be assigned to the substituted picolyl nitrogen.

The species distribution diagrams (**Figs. S10**) highlight that for both L^{3py} and L^{2S} the prevailing species at physiological pH (7.4) is HL^-, *i.e.* the *mono*-protonated form. This is consistent with the chemical composition estimated from ICP-MS and elemental analysis of the product which is isolated from neutral solution ($NaHL^{2S}$).

Table 1
Acidity constants (pK_a) of no3py (L^{3py}) and L^{2S} ($T = 25$ °C, $I = 0.1$ M NaCl). The reported uncertainty values were obtained by the fitting procedure and represent one standard deviation unit. *For clarity, the net charge of the ligand (L = L^{3py}, L^{2S}) and its protonated forms are omitted in the equilibria.

Equilibrium Reaction*	L^{3py}			L^{2S}	
		Potentiometry (a)	*UV–vis* (b)	*UV–vis*	*NMR*
$HL \rightleftharpoons H^+ + L$	$pK_{a,4}$	11.07	11.25	11.35 ± 0.06	10.79 ± 0.21
$H_2L \rightleftharpoons H^+ + HL$	$pK_{a,3}$	5.07	4.77	4.64 ± 0.02	4.51 ± 0.03
$H_3L \rightleftharpoons H^+ + H_2L$	$pK_{a,2}$	3.55	3.50	1.90 ± 0.08	1.90 ± 0.33
$H_4L \rightleftharpoons H^+ + H_3L$	$pK_{a,1}$	1.78	<2	–	–

[a] $T = 25$ °C; I 0.10 M KNO_3, taken from ref [21].
[b] $T = 25$ °C; I 0.10 M NaCl, taken from ref [30].

3.3. Kinetics, thermodynamic stability and inertness of [CuL^{2S}] in aqueous solution

The Cu(II)-L^{2S} system was firstly investigated in solution by means of high-resolution mass spectrometry (HR-MS) that confirmed the formation of the 1-to-1 metal-to-ligand complex [CuL^{2S}] with the characteristic isotopic pattern (**Fig. S11**). Complex formation was subsequently monitored by UV–Vis spectroscopy.

Addition of Cu(II) to a solution of the chelator in equimolar ratio causes an increase in the intensity of the main absorption at λ_{max} 263 nm, together with the appearance of a shoulder at 300 nm. These findings confirm the coordination of the pyridyl nitrogen atoms to Cu(II) (Fig. 6A). When Cu(II) is added to the free ligand buffered solution (PBS, pH 7.4), a d-d absorption band is formed at 685 nm, reaching its maximum at metal-to-ligand 1-to-1 M ratio (Fig. 6B).

The formation kinetics of the Cu(II)-L^{2S} complexes were qualitatively investigated using UV–Vis spectroscopy at different pH to assess the time needed to reach equilibrium. This study provides preliminary information on the binding ability of the chelator fundamental to collect accurate thermodynamic data, especially for macrocyclic ligands that may be characterized by slow complexation rates. The experiments were performed by monitoring over time the changes on the UV–Vis spectrum of the free-ligand after metal addition, until reaching the equilibrium. The complex formation was investigated by UV–Vis spectroscopy in three different media: PBS pH 7.4, 1.0 M HCl and 2.5 M HCl at 25 °C. The first one was chosen in representation of physiological fluids and the other two were considered as challenging media to test the competition between protons and copper for the ligand. The absorption spectrum of the [CuL^{2S}] complex isolated in the solid state was acquired in the same conditions and used as a reference to verify that the equilibrium was reached (**Fig. S12**).

The complex formation is almost instantaneous in PBS (pH 7.4), while it takes ~30 min in HCl, both 1 M and 2.5 M. It is notable to observe that the formation of the complex in such acidic conditions indicates a strong affinity of the chelator for the metal ion Cu(II).

In order to determine the speciation of the Cu(II)-L^{2S} system and the thermodynamic constants, the stability of the [CuL^{2S}] complex was investigated by UV–Vis spectroscopy in a wide pH range (0–12) (**Fig. S13**). No significant spectral changes are observed suggesting a very high stability of the [CuL^{2S}] species, as well as the absence of other complexes with different stoichiometries or protonation states, over a wide pH range (0–12). However, this behavior prevents the accurate calculation of the overall stability constant of the metal-complex system. Nonetheless, it is possible to estimate the minimum value of the stability constant for the species [CuL] ($\beta_{110(min)}$) by performing iterative fittings using progressively lower values of the stability constant. The lowest value that still provided an acceptable fit to the experimental data, without predicting any significant formation of free metal and ligand species, was taken as the minimum stability constant. The minimum value of pCu^{2+} ($-\log[Cu^{2+}]_{free}$) was obtained by simulating the species distribution curves with specific software programs such as PyES [34] and Hyss [54] (Table 2).

The estimated minimum pCu^{2+} value for L^{2S} is significantly higher than those reported in the literature for other polyazamacrocycles such as H_4TETA (15.1 [15]), H_4DOTA (17.6 [13]) and H_3NOTA (18.4 [15,17]). Although this minimum value is slightly lower than that estimated for the reference chelator no3py (L^{3py}), both values represent lower bounds, and the actual thermodynamic stability may be comparable.

In addition to thermodynamic stability, the inertness of the metal complex is fundamental for clinical applications. This can be assessed by monitoring changes in the primary coordination sphere of the metal ion

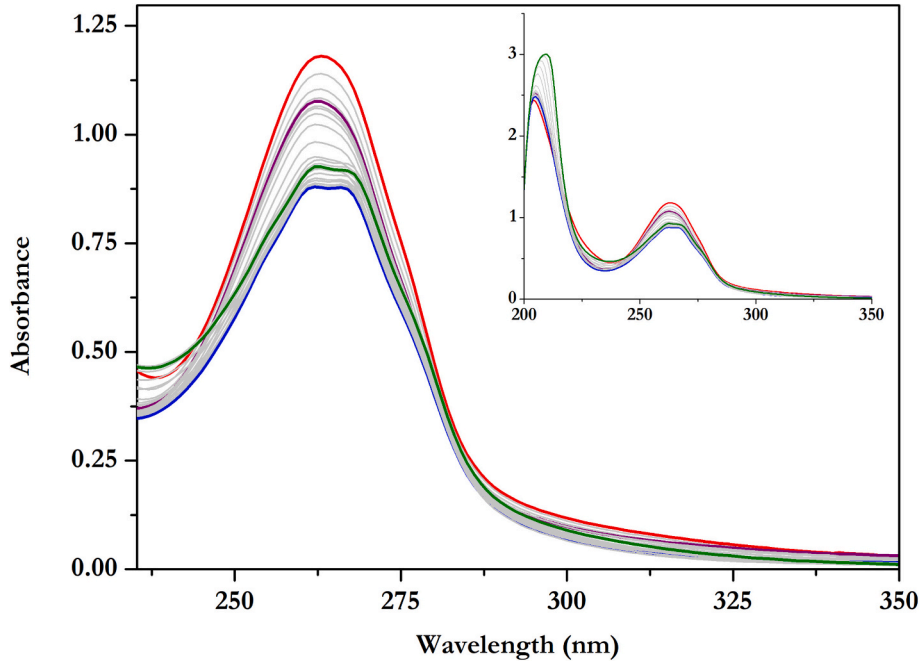

Fig. 5. Representative UV–Vis spectra of L^{2S} at different pH and spectra of the different protonated species: red curve (pH 1.5, H_3L^+); purple curve (pH 3.2; H_2L); blue curve (pH 8; HL^-); green curve (pH 12; L^{2-}) ($C_{L2S} = 0.1$ mM, $I = 0.1$ M NaCl, $T = 25$ °C). (For interpretation of the references to colour in this figure legend, the reader is referred to the web version of this article.)

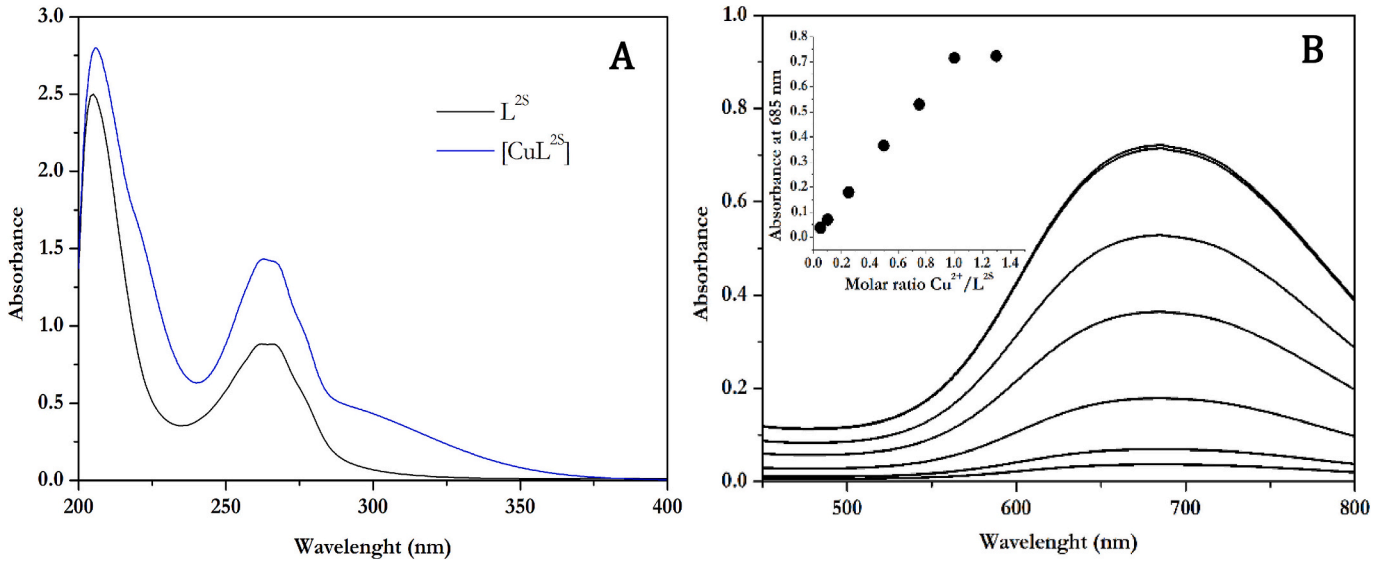

Fig. 6. A) UV–Vis spectra of L^{2S} (black) and the Cu(II)-L^{2S} system (blue) ($C_{Cu^{2+}} = C_{L2S} = 0.1$ mM; $I = 0.1$ M NaCl; pH = 7.4; $T = 25$ °C); **B)** Absorption visible spectra of L^{2S} upon increasing addition of Cu(II) together with the plot of absorbance at λ_{max} (685 nm) *vs.* Cu(II)/L^{2S} molar ratio ($C_{L2S} = 10$ mM; $I = 0.1$ M NaCl; pH = 7.4; $T = 25$ °C). (For interpretation of the references to colour in this figure legend, the reader is referred to the web version of this article.)

Table 2
Calculated minimum value of the overall stability constant for the species [CuL^{2S}] ($C_{Cu^{2+}} = C_{L^{2S}} = 10^{-4}$ M) and the corresponding minimum value of pCu^{2+} ($C_{CuL^{2S}} = 10C_{Cu^{2+}} = 10$ μM; pH 7.4) in comparison to the data reported in literature for L^{3py}. *(* Calculated minimum values; ** $\log\beta_{110}$ taken from reference [21] and pCu^{2+} value refers to $C_{CuL^{3py}} = 10C_{Cu^{2+}} = 10$ μM and pH 7.4).*

	$L^{2S(*)}$	$L^{3py(**)}$
$\log\beta_{110}$	26	27.4
pCu^{2+}	23	24

in the presence of highly concentrated acid solutions. As stated above, the formation of [CuL^{2S}] was observed in 1 M and 2.5 M HCl solutions, and when the solid complex is directly dissolved in the same media, it remains unchanged over a long time (1 week) at RT. As shown in **Fig. S14,** the *d-d* absorption band typical of the Cu(II)-complex is present, however, when the HCl concentration is increased to 5 M, a hypsochromic shift is observed (λ_{max} (PBS, pH 7.4) = 685 nm; λ_{max} (HCl 1 M) = 682 nm; λ_{max} (HCl 5 M) = 614 nm). As previously reported [55], this shift together with the decrease in absorbance upon increasing HCl concentration (1 M → 5 M) suggests that both chloride and [H^+] are involved in the reaction with the metal complex, possibly with the formation of the [$CuHL^{2S}Cl$] species. Despite the extremely harsh

conditions, no further changes are observed in absorption spectra over time up to 1 week (**Fig. S15**), suggesting that the equilibrium is quickly reached, that the chelator L^{2S} has high affinity for Cu(II) and demetallation likely does not occur. These results are fully consistent with those observed for TACN derivatives containing two pycolyl or thiazolyl pendant arms [55].

3.4. Structural characterization

DFT calculations (TPSSh/def2-TZVPP) allowed to investigate the geometry in aqueous solution of the [CuL^{2S}] complex and provided two energy minima corresponding to the diastereoisomeric forms Δ(λλλ) and Λ(λλλ) (Fig. 7**, Table S1**). The copper(II) coordination with L^{2S} resembles that of the parent ligand L^{3py} [21]. Two sources of helicity are present in this type of complexes: one related to the conformation of the three five-membered chelate rings formed upon the coordination of the TACN moiety (δ or λ), and the second linked to the two possible orientations of the three pendant arms of the ligand (Δ or Λ) [56,57]. As previously described [21], four possible stereoisomers which exist as two enantiomeric pairs can be formed: the Λ(λλλ)/Δ(δδδ) and Δ(λλλ)/Λ(δδδ) enantiomeric pairs. The calculated structures indicate that the two diastereoisomeric forms of the complexes show a rather broad range of Cu—N distances, a situation that can be attributed to Jahn-Teller distortions (Fig. 7).

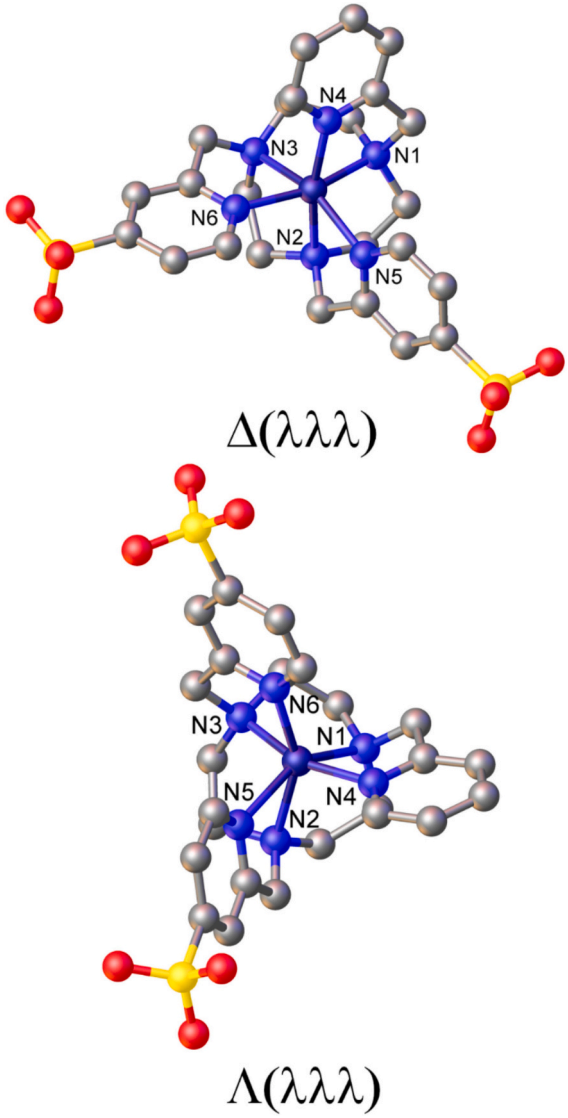

Fig. 7. TPSSH-D3-optimized structures of the Δ(λλλ) (bond distances: Cu—N1, 2.055; Cu—N2, 2.123; Cu—N3, 2.294; Cu—N4, 2.021; Cu—N5, 2.255; Cu—N6, 2.034 Å) and Λ(λλλ) (bond distances: Cu—N1, 2.175; Cu—N2, 2.258; Cu—N3, 2.035; Cu—N4, 2.012; Cu—N5, 2.271; Cu—N6, 2.076 Å) isomers of [CuL^{2S}].

The coordination geometry of the two [CuL^{2S}] diastereoisomers obtained with DFT calculations was examined using shape measures (Table 3 and **Fig. S16**). Shape measures provide an indication on how close a coordination environment is to the reference polyhedron, with a value of zero indicating a perfect match. The enantiomeric couple Δ(λλλ)/Λ(δδδ) is characterized by a slightly distorted octahedral geometry, while the Λ(λλλ)/Δ(δδδ) shows a coordination geometry that is close to a trigonal prism, as shown in Fig. 7 [58]. The shape measures calculated fall close to the minimal distortion path that relates an octahedron and a trigonal prism (**Fig. S16**, [59]).

DFT calculations afford a free energy difference between the two isomers (Δ(λλλ) and Λ(λλλ)) of only 0.04 kcal mol^{-1}, suggesting that at RT both the Δ(λλλ) and Λ(λλλ) species could be reasonably populated.

The EPR spectrum recorded from a frozen solution of [CuL^{2S}] at 77 K (Fig. 8) indeed indicates the presence of two species, with spectral deconvolution affording populations of 87% (major isomer) and 13% (minor isomer). Spectral simulations show that the major species is characterized by a rhombic g-tensor with $g_3 > (g_2 + g_1)/2 > 2$. This relation of g values is typical of mononuclear Cu(II) complexes with Jahn-Teller distortion and axial elongation, which results in a d_{x2-y2} ground state [60]. These spectral features allowed us to assign the major isomer to the Δ(λλλ)/Λ(δδδ) enantiomeric pair. Furthermore, the g_3/A_3 ratio of 149 cm is close to the range predicted for CuN_4 complexes with either square-planar or tetragonally distorted octahedral structures (100–145 cm) [61]. The g values for the minor isomer hint a more distorted geometry that can match with the isomeric couple Λ(λλλ)/Δ(δδδ) consistently with the shape analysis. A remarkable feature of the EPR spectrum of the minor species is the low A_3 value.

Electron paramagnetic resonance (EPR) measurements by Guillou et al. [21] revealed that $[CuL^{3py}]^{2+}$ predominantly adopts the distorted Λ(λλλ)/Δ(δδδ) isomeric form (76%), with only a minor population of the octahedral Δ(λλλ)/Λ(δδδ) configuration (24%). This isomeric distribution is further supported by the crystal structure reported by Han W. et al. [62], which confirms the presence of the Λ(λλλ)/Δ(δδδ) species. In contrast, the L^{2S} chelator exhibits a reversed isomeric preference, suggesting that the sulfonic substituents play a key role in modulating the equilibrium between these stereoisomeric forms.

The chemical structure of [CuL^{2S}] was investigated in the solid state by X-ray crystallography. However, the poor quality of the crystallographic data did not allow for a proper refinement of the structure. Nevertheless, the obtained crystal structure confirmed the tendency of copper(II) to form distorted octahedral complexes (**Figs. S17** and **S18, Table S3**).

3.5. Toward radiopharmaceutical applications

A copper-based complex aimed to clinical applications should be

Table 3
Shape analysis [50] together with the g- and A-tensors calculated from EPR data of [CuL^{2S}]. isomers.

	Isomer 1 Δ(λλλ)/Λ(δδδ)	Isomer 2 Λ(λλλ)/Δ(δδδ)
Octahedron (O_h)	1.91	4.97
Trigonal prism (D_{3h})	10.49	4.86
g1	2.08	2.02
g2	2.03	2.14
g3	2.29	2.28
A1	14.6	154.3
A2	44.8	−3.7
A3	460.2	234.1
Ratio (%)	86.6	13.4

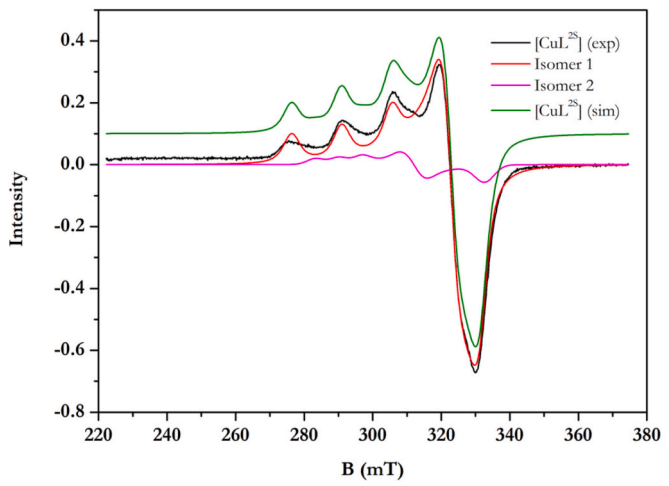

Fig. 8. Experimental EPR spectrum of [CuL^{2S}] in frozen solution (black), deconvoluted EPR spectra for isomer 1 (red) and isomer 2 (purple) together with simulated EPR spectrum (green) ($C_{CuL^{2S}}$ = 1 mM). (For interpretation of the references to colour in this figure legend, the reader is referred to the web version of this article.)

stable under reducing conditions in physiological environments to avoid redox-induced demetallation processes. Two factors concur to this, namely, a decrease of the reduction potential $E_{Cu^{2+}/Cu^{+}}$ below the threshold limit of reducing agents present *in vivo* (−605 mV *vs.* Ag/AgCl [63]) and a high affinity of the chelator for both oxidation states of copper ions. Cyclic voltammetry (CV) was employed to investigate the redox behavior of [CuL^{2S}], in sodium acetate (pH 4.5) (Fig. 9). Scan rate-dependent CV profiles confirmed diffusion-controlled electron transfer, excluding surface adsorption and validating solution-phase homogeneity (**Fig. S19**).

Voltammograms exhibited well-defined redox couples with peak separation indicative of *quasi*-reversible behavior ($\Delta E = E_{ox} - E_{red}$ = 82 mV). The $E_{1/2}$ value ($E_{1/2} = (E_{ox} + E_{red})/2$) for [CuL^{2S}] is −614 mV. The presence of sulfonic substituents affects the behavior of [CuL^{2S}] in comparison to [CuL^{3py}]$^{2+}$, with the former showing a less negative redox potential (−614 mV *vs.* -696 mV [21]) although almost equivalent ΔE value (82 mV *vs.* 91 mV [30]). These outcomes indicate a modest stabilization of the Cu(I) state while preserving quasi-reversible redox behavior. In addition, the $E_{1/2}$ value ($E_{1/2} \sim E_0$) remains slightly below the estimated reduction potential of common biological reductants (−605 mV *vs.* Ag/AgCl/3 M KCl [63]), suggesting a limited propensity for Cu(II) reduction under physiological conditions. The quasi-reversibility of the voltammogram of [CuL^{2S}] further supports its potential to trap Cu(I) in the time scale of the electrochemical experiment, offering a promising strategy to prevent demetallation and mitigate free copper release in biological environments.

Finally, to assess the ability of L^{2S} to chelate [^{64}Cu]Cu^{2+} under extremely dilute conditions, a radiolabeling investigation was conducted to explore the impacts of temperature, pH, and chelator concentration on the radiochemical incorporation (RCI) determined by radio-TLC analysis. Experiments were carried out in parallel using NODAGA as reference [64–66]. As shown in Fig. 10, at RT (pH = 4.5 and 7.0), L^{2S} is able to quantitatively incorporate [^{64}Cu]Cu^{2+} (RCI > 99%) in 10 min even at low concentration (10^{-6} M). The RCI slightly decreases by lowering the chelator concentration to 10^{-7} M (>90% pH 4.5; >79% at pH 7.0). On the other hand, the radiolabeling performances of NODAGA are appreciably poorer, as complete RCI is achieved only at a 100-fold higher concentration (10^{-5} M).

When the temperature is increased to 90 °C, the performances of both chelators remained almost unchanged. Even the variation in pH from a mildly acidic (pH 4.5) to a neutral environment (pH 7.0) did not significantly change the RCI for L^{2S}, although at low concentration (10^{-7} M) some hydrolysis phenomena may be competitive and reduce the metal incorporation (−12% RT, −32% 90 °C at pH 7.0 compared to pH 4.5). On the other hand, NODAGA showed a minimal increased chelating ability when the pH is raised to 7, nonetheless the RCI remains much lower compared to L^{2S} (5% at 10^{-6} M RT, 4% at 10^{-7} M RT).

The stability of [^{64}Cu][CuL^{2S}] in human serum (Fig. 11) was assessed to evaluate its structural integrity under physiological conditions, where endogenous ligands and metal ions may induce transchelation and transmetalation, potentially leading to *in vivo* demetallation. Both [^{64}Cu][Cu(NODAGA)]$^{-}$ and [^{64}Cu][CuL^{2S}] remained intact in human serum for up to 2 h, indicating good short-term stability under physiological conditions.

Overall, the chelator L^{2S} exhibits superior radiolabeling performance

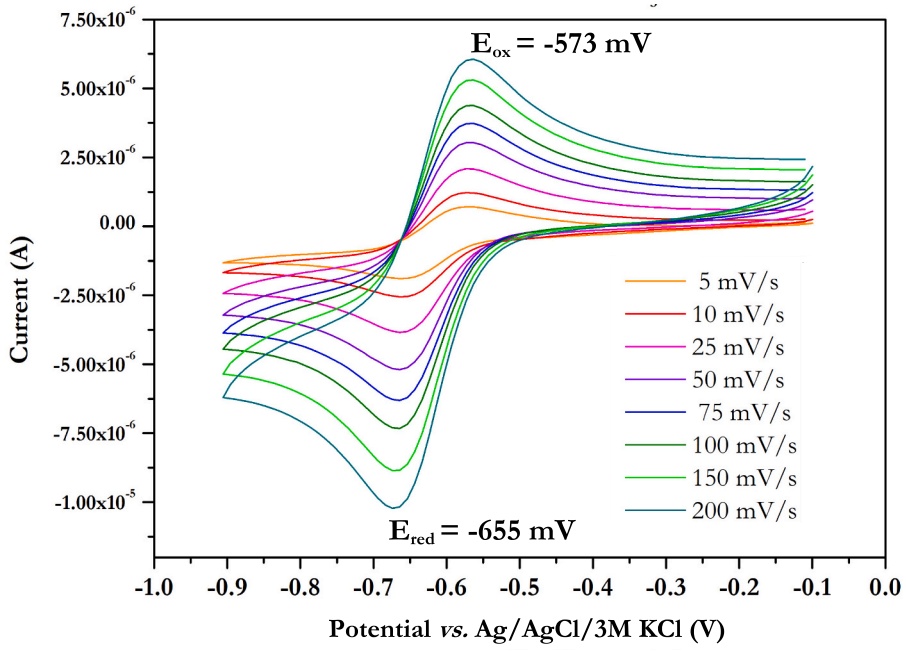

Fig. 9. Cyclic voltammograms of Cu-L^{2S} system ($C_{Cu^{2+}} = C_{L^{2S}}$ = 1 mM) at different scan rates in buffered aqueous solution (C_{CH_3COONa} = 0.1 M, pH = 4.5, T = 25 °C).

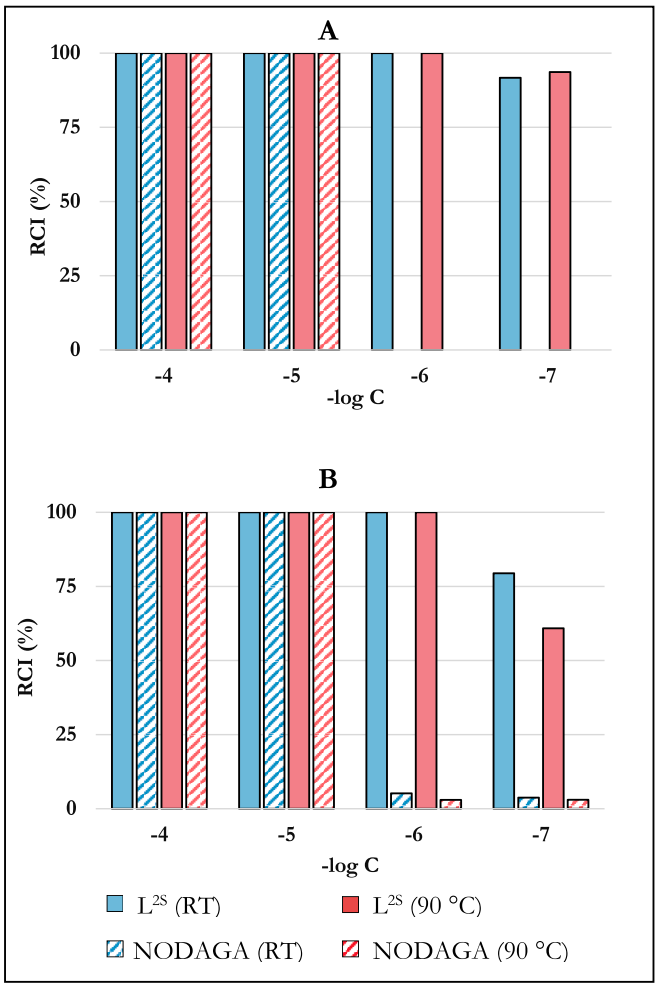

Fig. 10. Concentration- and temperature-dependent $[^{64}Cu]Cu^{2+}$ radiochemical incorporation (RCI, %) of L^{2S} and NODAGA at pH 4.5 (**A**) and 7.0 (**B**).

compared to NODAGA. Notably, it enables complete radiochemical incorporation at low concentrations (10^{-6} M) under mild conditions (pH 4.5, RT, 10 min), a feature of particular relevance for future radiopharmaceutical applications. This mild labeling protocol is especially advantageous when conjugating L^{2S} to a targeting vector, typically a biomolecule such as a peptide or antibody, which is often sensitive to elevated temperatures and harsh pH environments.

4. Conclusions

The development of copper(II) chelators combining rapid complexation at room temperature, high thermodynamic stability, and robustness upon reduction remains a central challenge in advancing copper-based radiopharmaceuticals. Here, we demonstrate that all three initial objectives were met: charge neutralization at physiological pH, preservation of no3py-like Cu(II) coordination properties, and highly efficient ^{64}Cu radiolabeling under mild conditions. This was achieved through the design and comprehensive characterization of a new TACN-derived ligand, L^{2S}, which retains the high-performance coordination behavior of the parent no3py framework while incorporating two non-coordinating sulfonate groups. This design enables enhanced aqueous solubility and neutralizes the global charge of the complex without compromising copper affinity, offering a level of tunability not accessible with classical TACN systems such as NOTA or NODAGA. L^{2S} displays acid–base properties closely aligned with no3py, forms highly stable Cu(II) complexes, and maintains structural integrity upon reduction to Cu(I), as demonstrated by cyclic voltammetry. Spectroscopic, crystallographic, and computational studies collectively revealed two stereoisomeric forms, with a predominant distorted-octahedral geometry (Δ(λλλ)/Λ(δδδ) pair). Importantly, $[CuL^{2S}]$ shows thermodynamic stability comparable to no3py and exceeds typical values reported for classical NOTA-based systems. Radiolabeling experiments highlight the practical relevance of this ligand, with quantitative $[^{64}Cu]Cu^{2+}$ incorporation achieved under mild conditions and at micromolar-to-submicromolar concentrations, outperforming the gold standard NODAGA. The radioactive complex also demonstrated excellent stability in human serum.

Altogether, these findings establish L^{2S} as a versatile platform for the development of bifunctional chelators for copper-based radiopharmaceutical applications.

CRediT authorship contribution statement

Matteo Mari: Writing – original draft, Methodology, Investigation, Formal analysis. **Véronique Patinec:** Writing – review & editing, Supervision, Data curation, Conceptualization. **Raúl Alvarado:** Data curation. **Sara Franchi:** Writing – review & editing, Investigation,

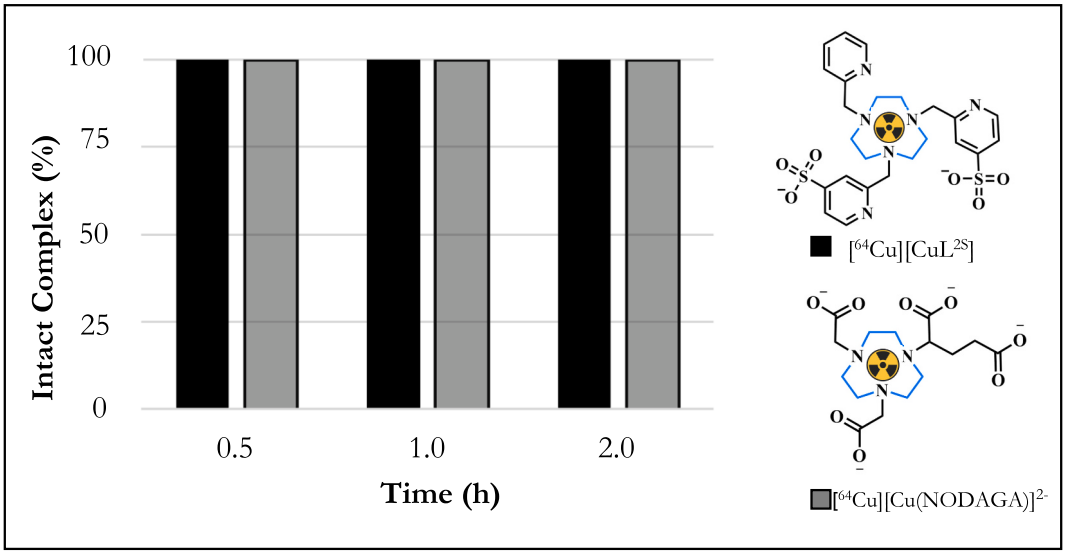

Fig. 11. Stability of $[^{64}Cu][CuL^{2S}]$ and $[^{64}Cu][Cu(NODAGA)]^{2-}$ in human serum (pH 7.4) at $T = 37$ °C.

Formal analysis. **Marianna Tosato:** Writing – review & editing, Investigation, Data curation. **Mattia Asti:** Writing – review & editing, Resources, Conceptualization. **Elia Frignani:** Formal analysis. **Laura Pigani:** Writing – review & editing, Data curation. **Jennifer Storchi:** Investigation. **Sven Stadlbauer:** Writing – review & editing, Resources. **Constantin Mamat:** Resources. **Klaus Kopka:** Writing – review & editing, Resources. **Marie Dallon:** Data curation. **Carlos Platas-Iglesias:** Writing – review & editing, Supervision, Methodology, Data curation. **Raphaël Tripier:** Writing – original draft, Resources, Project administration, Funding acquisition, Data curation, Conceptualization. **Erika Ferrari:** Writing – review & editing, Writing – original draft, Supervision, Project administration, Data curation, Conceptualization.

Declaration of competing interest

The authors declare that they have no known competing financial interests or personal relationships that could have appeared to influence the work reported in this paper.

Acknowledgments

The work was supported by the "FONDO DI ATENEO PER LA RICERCA 2024 - FAR2024 FOMO per progetti di ricerca interdisciplinari" (DR 1307/2024, Prot n. 323715, CUP E53C24003620007). M.M. and E.F. thank the Fondazione di Modena (https://www.fondazionedimodena.it) for financially supporting the project. The work was partly supported by the Italian Ministry of Health - Ricerca Corrente Annual Program 2025 (M.A.), AUSL-IRCCS Reggio Emilia (Italy). The authors would like to show gratitude the "Centro Interdipartimentale Grandi Strumenti - C.I.G.S." of the University of Modena and Reggio Emilia (https://www.cigs.unimore.it) for NMR, mass spectrometers and their precious technical support. The authors gratefully acknowledge the Université de Bretagne Occidentale for hosting M.M. during his doctoral mobility, supported by the "Incoming mobility grants for international PhD students in Brittany" program (UBO-DEVE, 2023 – Call 1). The authors also thank the Erasmus+ program and the interinstitutional partnership between UNIMORE and UBO for facilitating this international research collaboration. The authors are thankful to the NECTAR Cost Action (CA 18202; https://www.cost-nectar.eu/) for collecting and analyzing equilibrium constants for hydrolysis and associated equilibria in critical compilations. The authors also thank Centro de Supercomputación de Galicia (CESGA) for providing access to supercomputing facilities.

Appendix A. Supplementary data

Supplementary data to this article can be found online at https://doi.org/10.1016/j.inoche.2026.116782.

Data availability

Data will be made available on request.

References

[1] B.J. Burkett, D.J. Bartlett, P.W. McGarrah, A.R. Lewis, D.R. Johnson, K. Berberoğlu, M.K. Pandey, A.T. Packard, T.R. Halfdanarson, C.B. Hruska, G.B. Johnson, A. T. Kendi, A review of Theranostics: perspectives on emerging approaches and clinical advancements, Radiol. Imaging Cancer 5 (2023), https://doi.org/10.1148/RYCAN.220157.

[2] C.J. Anderson, R. Ferdani, Copper-64 radiopharmaceuticals for PET imaging of Cancer: advances in preclinical and clinical research, Cancer Biother. Radiopharm. 24 (2024) 379–393, https://doi.org/10.1089/cbr.2009.0674.

[3] C.A. Boswell, X. Sun, W. Niu, G.R. Weisman, E.H. Wong, A.L. Rheingold, C. J. Anderson, Comparative in vivo stability of Copper-64-Labeled cross-bridged and conventional Tetraazamacrocyclic complexes, J. Med. Chem. 47 (2004) 1465–1474, https://doi.org/10.1021/jm030383m.

[4] M. Tosato, S. Franchi, A.A. Isse, A. Del Vecchio, G. Zanoni, A. Alker, M. Asti, T. Gyr, V. Di Marco, H. Mäcke, Is smaller better? Cu^{2+}/Cu^{+} coordination chemistry and Copper-64 radiochemical investigation of a 1,4,7-Triazacyclononane-based Sulfur-rich Chelator, Inorg. Chem. 62 (2023) 20621–20633, https://doi.org/10.1021/acs.inorgchem.3c00621.

[5] G. Hao, T. Mastren, W. Silvers, G. Hassan, O.K. Öz, X. Sun, Copper-67 radioimmunotheranostics for simultaneous immunotherapy and immuno-SPECT, Sci. Rep. 11 (2021) 1–11, https://doi.org/10.1038/s41598-021-82812-1.

[6] A. Pfeifer, U. Knigge, J. Mortensen, P. Oturai, A.K. Berthelsen, A. Loft, T. Binderup, P. Rasmussen, D. Elema, T.L. Klausen, S. Holm, E. Von Benzon, L. Højgaard, A. Kjaer, Clinical PET of neuroendocrine Tumors using 64Cu-DOTATATE: first-in-humans study, J. Nucl. Med. 53 (2012) 1207–1215, https://doi.org/10.2967/JNUMED.111.101469.

[7] C.B. Johnbeck, U. Knigge, A. Loft, A.K. Berthelsen, J. Mortensen, P. Oturai, S. W. Langer, D.R. Elema, A. Kjaer, Head-to-head comparison of ^{64}Cu-DOTATATE and ^{68}Ga-DOTATOC PET/CT: a prospective study of 59 patients with neuroendocrine Tumors, J. Nucl. Med. 58 (2017) 451–457, https://doi.org/10.2967/JNUMED.116.180430.

[8] C.F. Ramogida, C. Orvig, Tumour targeting with radiometals for diagnosis and therapy, Chem. Commun. 49 (2013) 4720–4739, https://doi.org/10.1039/C3CC41554F.

[9] L.M.P. Lima, D. Esteban-Gómez, R. Delgado, C. Platas-Iglesias, R. Tripier, Monopicolinate cyclen and cyclam derivatives for stable copper(II) complexation, Inorg. Chem. 51 (2012) 6916–6927, https://doi.org/10.1021/IC300784V.

[10] L.M.P. Lima, Z. Halime, R. Marion, N. Camus, R. Delgado, C. Platas-Iglesias, R. Tripier, Monopicolinate cross-bridged cyclam combining very fast complexation with very high stability and inertness of its copper(II) complex, Inorg. Chem. 53 (2014) 5269–5279, https://doi.org/10.1021/ic500491c.

[11] M. Tosato, M. Pelosato, S. Franchi, A.A. Isse, N.V. May, G. Zanoni, F. Mancin, P. Pastore, D. Badocco, M. Asti, V. Di Marco, When ring makes the difference: coordination properties of cu^{2+}/Cu^{+} complexes with sulfur-pendant polyazamacrocycles for radiopharmaceutical applications, New J. Chem. 46 (2022) 10012–10025, https://doi.org/10.1039/d2nj01032a.

[12] M. Roger, L.M.P. Lima, M. Frindel, C. Platas-Iglesias, J.F. Gestin, R. Delgado, V. Patinec, R. Tripier, Monopicolinate-dipicolyl derivative of triazacyclononane for stable complexation of Cu^{2+} and $^{64}Cu^{2+}$, Inorg. Chem. 52 (2013) 5246–5259, https://doi.org/10.1021/ic400174r.

[13] M. Tosato, M. Dalla Tiezza, N.V. May, A.A. Isse, S. Nardella, L. Orian, M. Verona, C. Vaccarin, A. Alker, H. MäcKe, P. Pastore, V. Di Marco, Copper coordination chemistry of Sulfur pendant Cyclen derivatives: an attempt to hinder the reductive-induced Demetalation in $^{64/67}$Cu radiopharmaceuticals, Inorg. Chem. 60 (2021) 11530–11547, https://doi.org/10.1021/ACS.INORGCHEM.1C01550.

[14] R. Gillet, A. Roux, J. Brandel, S. Huclier-Markai, F. Camerel, O. Jeannin, A. M. Nonat, L.J. Charbonnière, A Bispidol Chelator with a phosphonate pendant arm: synthesis, cu(II) complexation, and ^{64}Cu Labeling, Inorg. Chem. 56 (2017) 11738–11752, https://doi.org/10.1021/acs.inorgchem.7b01731.

[15] T.J. Wadas, E.H. Wong, G.R. Weisman, C.J. Anderson, Coordinating Radiometals of Copper, Gallium, Indium, Yttrium, and Zirconium for PET and SPECT Imaging of Disease, 2026, https://doi.org/10.1021/cr900325h.

[16] L. Wei, Y. Ye, T.J. Wadas, J.S. Lewis, M.J. Welch, S. Achilefu, C.J. Anderson, ^{64}Cu-Labeled CB-TE2A and Diamsar conjugated RGD peptide Analogs for targeting angiogenesis: comparison of their biological activity, Nucl. Med. Biol. 36 (2009) 277, https://doi.org/10.1016/J.NUCMEDBIO.2008.12.008.

[17] E. Boros, A.B. Packard, Radioactive transition metals for imaging and therapy, Chem. Rev. 119 (2019) 870–901, https://doi.org/10.1021/ACS.CHEMREV.8B00281.

[18] V. Kubíček, Z. Böhmová, R. Ševčíková, J. Vaněk, P. Lubal, Z. Poláková, R. Michalicová, J. Kotek, P. Hermann, NOTA complexes with copper(II) and divalent metal ions: kinetic and thermodynamic studies, Inorg. Chem. 57 (2018) 3061–3072, https://doi.org/10.1021/ACS.INORGCHEM.7B02929.

[19] R. Ševčík, J. Vaněk, R. Michalicová, P. Lubal, P. Hermann, I.C. Santos, I. Santos, M. P.C. Campello, Formation and decomplexation kinetics of copper(II) complexes with cyclen derivatives having mixed carboxylate and phosphonate pendant arms, Dalton Trans. 45 (2016) 12723–12733, https://doi.org/10.1039/C6DT01127F.

[20] A. Ahmedova, B. Todorov, N. Burdzhiev, C. Goze, Copper radiopharmaceuticals for theranostic applications, Eur. J. Med. Chem. 157 (2018) 1406–1425, https://doi.org/10.1016/J.EJMECH.2018.08.051.

[21] A. Guillou, L.M.P. Lima, M. Roger, D. Esteban-Gómez, R. Delgado, C. Platas-Iglesias, V. Patinec, R. Tripier, 1,4,7-Triazacyclononane-based bifunctional picolinate ligands for efficient copper complexation, Eur. J. Inorg. Chem. 2017 (2017) 2435–2443, https://doi.org/10.1002/ejic.201700176.

[22] A. Marlin, I. Hierlmeier, A. Guillou, M. Bartholomä, R. Tripier, V. Patinec, Bioconjugated chelates based on (methylpyridinyl)tacn: synthesis, 64Cu labeling and in vitro evaluation for prostate cancer targeting, Metallomics 14 (2022) 36, https://doi.org/10.1093/mtomcs/mfac036.

[23] J. Dearling, B. Paterson, P. Dunning, E. Snay, S.T. Treves, S. Voss, P. Donnelly, A. Packard, The effect of chelator charge on the biodistribution of engineered antibodies labeled with ^{64}Cu, J. Nucl. Med. 54 (2013) 1090, https://jnm.snmjournals.org/content/54/supplement_2/1090.

[24] G. Selvi, F.A. Özdemir, G. Aykutoglu, N. Özdemir, Z. Şerbetçi, B. Çetinkaya, O. Dayan, A neutral arene ruthenium(II) complex with a sulfonated N,O-chelating ligand: Synthesis, characterization, in vitro cytotoxicity and antibacterial activity, Polyhedron 176 (2020) 114300, https://doi.org/10.1016/J.POLY.2019.114300.

[25] J. Canivet, G. Süss-Fink, Water-soluble arene ruthenium catalysts containing sulfonated diamine ligands for asymmetric transfer hydrogenation of α-aryl ketones and imines in aqueous solution, Green Chem. 9 (2007) 391–397, https://doi.org/10.1039/B612518B.

[26] S. García-Gallego, J.S. Rodríguez, J.L. Jiménez, M. Cangiotti, M.F. Ottaviani, M.Á. Muñoz-Fernández, R. Gómez, F.J. De La Mata, Polyanionic N-donor ligands as chelating agents in transition metal complexes: synthesis, structural characterization and antiviral properties against HIV, Dalton Trans. 41 (2012) 6488–6499, https://doi.org/10.1039/C2DT11793B.
[27] J. Salaam, G. Pilet, J. Hasserodt, Multiple sulfonation of Picolyl-based complexes rendering them highly water-compatible, Inorg. Chem. 59 (2020) 13812–13816, https://doi.org/10.1021/ACS.INORGCHEM.0C02017.
[28] S. Stoll, A. Schweiger, EasySpin, a comprehensive software package for spectral simulation and analysis in EPR, J. Magn. Reson. 178 (2006) 42–55, https://doi.org/10.1016/J.JMR.2005.08.013.
[29] F. Molton, Simultispin: a versatile graphical user interface for the simulation of solid-state continuous wave EPR spectra, Magn. Reson. Chem. 58 (2020) 718–726, https://doi.org/10.1002/MRC.5019.
[30] M. Mari, S. Belluti, L. Pampanella, C. Imbriano, A. Zambon, J. Storchi, L. Pigani, M. Tosato, S. Rubagotti, P.C. Capponi, M. Asti, V. Patinec, R. Tripier, E. Ferrari, Targeting monocarboxylate transporter 1 with a copper-chelating coumarin-based bioconjugate: synthesis and characterization, J. Inorg. Biochem. 275 (2026) 113130, https://doi.org/10.1016/J.JINORGBIO.2025.113130.
[31] A.K. Covington, M. Paabo, R.A. Robinson, R.G. Bates, H. Hyman, A. Kaganove, J. J. Katz, N.C. Li, P. Tang, R. Mathur, Use of the glass electrode in deuterium oxide and the relation between the standardized pD (paD) scale and the operational pH in heavy Water. https://pubs.acs.org/sharingguidelines, 1962.
[32] M. Tosato, M. Boniburini, F. Faglioni, F. Genua, M. Mari, J. Storchi, S. Franchi, M. Asti, E. Ferrari, Thwarting isomerization through rigidity: a promising HBED derivative for the chelation of Gallium-68, Inorg. Chem. 64 (2025) 18673–18686, https://doi.org/10.1021/ACS.INORGCHEM.5C00930.
[33] P. Gans, A. Sabatini, A. Vacca, Investigation of equilibria in solution. Determination of equilibrium constants with the HYPERQUAD suite of programs, Talanta 43 (1996) 1739–1753, https://doi.org/10.1016/0039-9140(96)01958-3.
[34] L. Castellino, E. Alladio, S. Bertinetti, G. Lando, C. De Stefano, S. Blasco, E. García-España, S. Gama, S. Berto, D. Milea, PyES – an open-source software for the computation of solution and precipitation equilibria, Chemometr. Intell. Lab. Sys. 239 (2023), https://doi.org/10.1016/j.chemolab.2023.104860.
[35] G.M. Sheldrick, SHELXT – integrated space-group and crystal-structure determination, Urn:Issn:2053–2733 71 (2015) 3–8, https://doi.org/10.1107/S2053273314026370.
[36] G.M. Sheldrick, Crystal structure refinement with SHELXL, Urn:Issn:2053–2296, Acta Crystallogr. Sect. C Struct. Chem. 71 (2015) 3–8, https://doi.org/10.1107/S2053229614024218.
[37] F. Neese, J. Wiley, The ORCA program system, Wiley Interdiscip. Rev. Comput. Mol. Sci. 2 (2012) 73–78, https://doi.org/10.1002/WCMS.81.
[38] F. Neese, Software update: the ORCA program system—version 6.0, WIREs Comput. Mol. Sci. 15 (2025), https://doi.org/10.1002/wcms.70019.
[39] F. Neese, The SHARK integral generation and digestion system, J. Comput. Chem. 44 (2023) 381–396, https://doi.org/10.1002/JCC.26942.
[40] F. Weigend, R. Ahlrichs, Balanced basis sets of split valence, triple zeta valence and quadruple zeta valence quality for H to Rn: design and assessment of accuracy, Phys. Chem. Chem. Phys. 7 (2005) 3297–3305, https://doi.org/10.1039/B508541A.
[41] S. Grimme, S. Ehrlich, L. Goerigk, Effect of the damping function in dispersion corrected density functional theory, J. Comput. Chem. 32 (2011) 1456–1465, https://doi.org/10.1002/JCC.21759.
[42] S. Grimme, J. Antony, S. Ehrlich, H. Krieg, A consistent and accurate ab initio parametrization of density functional dispersion correction (DFT-D) for the 94 elements H-Pu, J. Chem. Phys. 132 (2010), https://doi.org/10.1063/1.3382344/926936.
[43] F. Neese, An improvement of the resolution of the identity approximation for the formation of the coulomb matrix, J. Comput. Chem. 24 (2003) 1740–1747, https://doi.org/10.1002/JCC.10318.
[44] F. Neese, F. Wennmohs, A. Hansen, U. Becker, Efficient, approximate and parallel Hartree–Fock and hybrid DFT calculations. A 'chain-of-spheres' algorithm for the Hartree–Fock exchange, Chem. Phys. 356 (2009) 98–109, https://doi.org/10.1016/J.CHEMPHYS.2008.10.036.
[45] D. Bykov, T. Petrenko, R. Izsák, S. Kossmann, U. Becker, E. Valeev, F. Neese, Efficient implementation of the analytic second derivatives of Hartree–Fock and hybrid DFT energies: a detailed analysis of different approximations, Mol. Phys. 113 (2015) 1961–1977, https://doi.org/10.1080/00268976.2015.1025114.
[46] B. Helmich-Paris, B. de Souza, F. Neese, R. Izsák, An improved chain of spheres for exchange algorithm, J. Chem. Phys. 155 (2021), https://doi.org/10.1063/5.0058766/1013244.
[47] G.L. Stoychev, A.A. Auer, F. Neese, Automatic generation of auxiliary basis sets, J. Chem. Theory Comput. 13 (2017) 554–562, https://doi.org/10.1021/ACS.JCTC.6B01041.
[48] M. Garcia-Ratés, F. Neese, Effect of the solute cavity on the solvation energy and its derivatives within the framework of the gaussian charge scheme, J. Comput. Chem. 41 (2020) 922–939, https://doi.org/10.1002/JCC.26139.
[49] A.V. Marenich, C.J. Cramer, D.G. Truhlar, Universal solvation model based on solute Electron density and on a continuum model of the solvent defined by the bulk dielectric constant and atomic surface tensions, J. Phys. Chem. B 113 (2009) 6378–6396, https://doi.org/10.1021/JP810292N.
[50] M. Llunell, D. Casanova, J. Cirera, J.M. Bofill, P. Alemany, S. Alvarez, M. Pinsky, D. D. Avnir, SHAPE v2.1, 2013.
[51] G. Gasser, L. Tjioe, B. Graham, M.J. Belousoff, S. Juran, M. Walther, J.U. Künstler, R. Bergmann, H. Stephan, L. Spiccia, Synthesis, copper(II) complexation, 64Cu-Labeling, and bioconjugation of a new bis(2-pyridylmethyl) derivative of 1,4,7-Triazacyclononane, Bioconjug. Chem. 19 (2008) 719–730, https://doi.org/10.1021/BC700396E.
[52] V. Stavila, M. Allali, L. Canaple, Y. Stortz, C. Franc, P. Maurin, O. Beuf, O. Dufay, J. Samarut, M. Janier, J. Hasserodt, Significant relaxivity gap between a low-spin and a high-spin iron(II) complex of structural similarity: an attractive off–on system for the potential design of responsive MRI probes, New J. Chem. 32 (2008) 428–435, https://doi.org/10.1039/B715254J.
[53] J.P. Guthrie, Hydrolysis of esters of oxy acids: pKa values for strong acids; Brønsted relationship for attack of water at methyl; free energies of hydrolysis of esters of oxy acids; and a linear relationship between free energy of hydrolysis and pKa holding over a ra 56, 2011, pp. 2342–2354, https://doi.org/10.1139/V78-385. Doi: https://doi.org/10.1139/V78-385.
[54] L. Alderighi, P. Gans, A. Ienco, D. Peters, A. Sabatini, A. Vacca, Hyperquad simulation and speciation (HySS): a utility program for the investigation of equilibria involving soluble and partially soluble species, Coord. Chem. Rev. 184 (1999) 311–318, https://doi.org/10.1016/S0010-8545(98)00260-4.
[55] R. Uzal-Varela, V. Patinec, R. Tripier, L. Valencia, M. Maneiro, M. Canle, C. Platas-Iglesias, D. Esteban-Gómez, E. Iglesias, On the dissociation pathways of copper complexes relevant as PET imaging agents, J. Inorg. Biochem. 236 (2022), https://doi.org/10.1016/J.JINORGBIO.2022.111951.
[56] J.J. Wilson, E.R. Birnbaum, E.R. Batista, R.L. Martin, K.D. John, Synthesis and characterization of nitrogen-rich macrocyclic ligands and an investigation of their coordination chemistry with lanthanum(III), Inorg. Chem. 54 (2015) 97–109, https://doi.org/10.1021/ic501843c.
[57] M. Regueiro-Figueroa, E. Ruscsák, L. Fra, G. Tircsõ, I. Tõth, A. De Blas, T. Rodríguez-Blas, C. Platas-Iglesias, D. Esteban-Gõmez, Highly stable complexes of divalent metal ions (Mg^{2+}, Ca^{2+}, Cu^{2+}, Zn^{2+}, Cd^{2+}, and Pb^{2+}) with a DOTA-like ligand containing a picolinate pendant, Eur. J. Inorg. Chem. 2014 (2014) 6165–6173, https://doi.org/10.1002/EJIC.201402693.
[58] S. Alvarez, D. Avnir, M. Llunell, M. Pinsky, Continuous symmetry maps and shape classification. The case of six-coordinated metal compounds, New J. Chem. 26 (2002) 996–1009, https://doi.org/10.1039/B200641N.
[59] D. Casanova, J. Cirera, M. Llunell, P. Alemany, D. Avnir, S. Alvarez, Minimal distortion pathways in polyhedral rearrangements, J. Am. Chem. Soc. 126 (2004) 1755–1763, https://doi.org/10.1021/JA036479N.
[60] J. Peisach, W.E. Blumberg, Structural implications derived from the analysis of electron paramagnetic resonance spectra of natural and artificial copper proteins, Arch. Biochem. Biophys. 165 (1974) 691–708, https://doi.org/10.1016/0003-9861(74)90298-7.
[61] B. Bennett, J.M. Kowalski, EPR methods for biological cu(II): L-band CW and NARS, Methods Enzymol. 563 (2015) 341–361, https://doi.org/10.1016/BS.MIE.2015.06.030.
[62] W. Han, Z.D. Wang, C.Z. Xie, Z.Q. Liu, S.P. Yan, D.Z. Liao, Z.H. Jiang, P. Cheng, Crystal structures and spectroscopic properties of copper(II) and zinc(II) complexes with the macrocycle 1,4,7-tris(2-pyridylmethyl)-1,4,7- triazacyclononane, J. Chem. Crystallogr. 34 (2004) 495–500, https://doi.org/10.1023/B:JOCC.0000042016.86927.1B.
[63] A. Rodríguez-Rodríguez, Z. Halime, L.M.P. Lima, M. Beyler, D. Deniaud, N. Le Poul, R. Delgado, C. Platas-Iglesias, V. Patinec, R. Tripier, Cyclams with ambidentate Methylthiazolyl pendants for stable, inert, and selective cu(II) coordination, Inorg. Chem. 55 (2016) 619–632, https://doi.org/10.1021/ACS.INORGCHEM.5B01779.
[64] S.C. Ghosh, K.L. Pinkston, H. Robinson, B.R. Harvey, N. Wilganowski, K. Gore, E. M. Sevick-Muraca, A. Azhdarinia, Comparison of DOTA and NODAGA as chelators for ^{64}Cu-labeled immunoconjugates, Nucl. Med. Biol. 42 (2015) 177–183, https://doi.org/10.1016/J.NUCMEDBIO.2014.09.009.
[65] N. Amraee, B. Alirezapour, M. Hosntalab, A. Hadadi, H. Yousefnia, Development of [^{64}Cu]cu-NODAGA-RGD-BBN as a novel radiotracer for dual integrin and GRPR-targeted tumor PET imaging, Curr. Radiopharm. 18 (2025) 37–44, https://doi.org/10.2174/0118744710246897240209070005.
[66] M. Shojaei, Q. Zhou, G. Palumbo, R. Schaefer, J. Kaskinoro, P. Vehmaan-Kreula, P. Bartenstein, M. Brendel, D. Edbauer, S. Lindner, Development and preclinical evaluation of a Copper-64-Labeled antibody targeting Glycine-alanine dipeptides for PET imaging of C9orf72-associated amyotrophic lateral sclerosis/frontotemporal dementia, ACS Pharmacol. Transl. Sci. 7 (2024) 1404–1414, https://doi.org/10.1021/ACSPTSCI.4C00037.

Erika Ferrari is Associate Professor of Inorganic Chemistry at the University of Modena and Reggio Emilia (UNIMORE), Italy. She received her Master's degree in Chemistry (*summa cum laude*) in 1999 and her Ph.D. in 2003, both from UNIMORE. Following a tenure as an Assistant Professor, she was appointed to her current role within the Department of Chemical and Geological Sciences in 2020. Prof. Ferrari's research is situated at the interface of coordination chemistry, bioinorganic chemistry, and medicinal inorganic chemistry. Her scientific program is characterized by a strong interdisciplinary approach to the design, synthesis, and thermodynamic characterization of metal-ligand systems derived from both natural and synthetic sources. Her early career contributions significantly advanced the development of curcumin-based metallodrugs, specifically addressing challenges in chemical stability and bioavailability for oncological applications. Over the past decade, her research has shifted toward the design of innovative radiopharmaceuticals for PET imaging and theranostics. This field involves the strategic use of various radiometals - including copper, gallium, scandium, silver, and lead - to develop targeting agents that integrate specific molecular vectors with therapeutic/diagnostic metal cores.

Prof. Raphaël Tripier obtained his Ph.D. in Chemistry from the University of Burgundy (Dijon, France) in 2000, working under the joint supervision of Prof. Robert Guilard and Prof. Franck Denat. He then pursued a postdoctoral fellowship at the École Polytechnique Fédérale de Lausanne (Lausanne, Switzerland), where he specialized in lanthanide-based supramolecular chemistry in the group of Prof. Jean-Claude G. Bünzli. In 2001, he joined the CNRS as a research scientist at the University of Brest (Université de Bretagne Occidentale), where he developed an independent research program at the interface of coordination chemistry and molecular imaging. He was promoted to Full Professor in 2011 and currently leads the MAC (Macrocycles And Coordination) research group within the CEMCA UMR 6521. His research activities are centered on the conception and synthesis of polyazamacrocyclic ligands and their metal complexes, with particular emphasis on copper and lanthanide systems for biomedical applications. His work integrates ligand design, coordination chemistry, and detailed physicochemical characterization, including thermodynamic stability, kinetic inertness, and structural analysis. These fundamental studies are closely connected to translational objectives, notably in molecular imaging modalities such as MRI and PET, as well as in theranostic approaches and targeted radiopharmaceutical development. More recently, his research has expanded toward the development of multifunctional and bifunctional chelators, enabling bioconjugation to peptides and antibodies, and the design of advanced probes for nuclear medicine and optical imaging. His contributions also include the exploration of structure–property relationships governing metal complex behavior in biological environments, with the aim of improving selectivity, stability, and in vivo performance.